Biochemical and structural basis of polyamine, lysine and ornithine acetylation catalyzed by spermine/spermidine N-acetyl transferase in moss and maize

Jakub Bělíček, Eva Ľuptáková, David Kopečný, Jan Frömmel, Armelle Vigouroux, Sanja Ćavar Zeljković, Franjo Jagic, Pierre Briozzo, David Jaroslav Kopečný, Petr Tarkowski, et al.

the plant journal

SEB SOCIETY FOR EXPERIMENTAL BIOLOGY

The Plant Journal (2023) **114,** 482–498 doi: 10.1111/tpj.16148

Biochemical and structural basis of polyamine, lysine and ornithine acetylation catalyzed by spermine/spermidine *N*-acetyl transferase in moss and maize

Jakub Bělíček[1,†], Eva Ľuptáková[1,†], David Kopečný[1], Jan Frömmel[2], Armelle Vigouroux[3], Sanja Ćavar Zeljković[2,4], Franjo Jagic[5], Pierre Briozzo[5], David Jaroslav Kopečný[1], Petr Tarkowski[2,4], Jaroslav Nisler[2,6], Nuria De Diego[2], Solange Moréra[3,*] and Martina Kopečná[1,*]

[1]*Department of Experimental Biology, Faculty of Science, Palacký University, Šlechtitelů 27, Olomouc CZ-78371, Czech Republic,*

[2]*Czech Advanced Technology and Research Institute, Palacký University, Šlechtitelů 27, CZ-78371, Olomouc, Czech Republic,*

[3]*CEA, CNRS, Université Paris-Saclay, Institute for Integrative Biology of the Cell (I2BC), F-91198, Gif-sur-Yvette, France,*

[4]*Department of Genetic Resources for Vegetables, Medicinal and Special Plants, Centre of the Region Haná for Biotechnological and Agricultural Research, Crop Research Institute, Šlechtitelů 29, CZ-78371, Olomouc, Czech Republic,*

[5]*INRAE, AgroParisTech, Université Paris-Saclay, Institut Jean-Pierre Bourgin (IJPB), Route de Saint Cyr, F-78026, Versailles, France, and*

[6]*Isotope Laboratory, Institute of Experimental Botany, The Czech Academy of Sciences, Vídeňská 1083, CZ-14220, Prague, Czech Republic*

Received 23 September 2022; accepted 8 February 2023; published online 14 February 2023.
*For correspondence (e-mail martina.kopecna@upol.cz; solange.morera@i2bc.paris-saclay.fr).
†These authors contributed equally to this work.

SUMMARY

Polyamines such as spermidine and spermine are essential regulators of cell growth, differentiation, maintenance of ion balance and abiotic stress tolerance. Their levels are controlled by the spermidine/spermine *N*^{1}-acetyltransferase (SSAT) via acetylation to promote either their degradation or export outside the cell as shown in mammals. Plant genomes contain at least one gene coding for SSAT (also named NATA for *N*-AcetylTransferase Activity). Combining kinetics, HPLC-MS and crystallography, we show that three plant SSATs, one from the lower plant moss *Physcomitrium patens* and two from the higher plant *Zea mays*, acetylate various aliphatic polyamines and two amino acids lysine (Lys) and ornithine (Orn). Thus, plant SSATs exhibit a broad substrate specificity, unlike more specific human SSATs (hSSATs) as hSSAT1 targets polyamines, whereas hSSAT2 acetylates Lys and thiaLys. The crystal structures of two PpSSAT ternary complexes, one with Lys and CoA, the other with acetyl-CoA and polyethylene glycol (mimicking spermine), reveal a different binding mode for polyamine versus amino acid substrates accompanied by structural rearrangements of both the coenzyme and the enzyme. Two arginine residues, unique among plant SSATs, hold the carboxyl group of amino acid substrates. The most abundant acetylated compound accumulated in moss was *N*^{6}-acetyl-Lys, whereas *N*^{5}-acetyl-Orn, known to be toxic for aphids, was found in maize. Both plant species contain very low levels of acetylated polyamines. The present study provides a detailed biochemical and structural basis of plant SSAT enzymes that can acetylate a wide range of substrates and likely play various roles *in planta*.

Keywords: acetylation, coenzyme A, lysine, *N*-acetyl transferase, ornithine, *Physcomitrium patens*, polyamine, spermine, X-ray crystallography, *Zea mays*.

INTRODUCTION

Polyamines, such as putrescine (1,4-diaminobutane, Put), spermine (Spm) and spermidine (Spd) are aliphatic nitrogenous polycations ubiquitously present in all cell types in plants and animals. They contain two or more amino groups with very potent biological activity. Indeed, abnormally high cellular polyamine levels in human cells are associated with diseases such as Alzheimer's, cystic fibrosis and cancer (Pegg, 2008; Perez-Leal & Merali, 2012; Wallace et al., 2003). Spm and Spd together are essential for

cell proliferation, growth and normal cellular homeostasis, and they can be found bound to RNA within cells. In plants, deficiency in polyamine biosynthesis leads to hypersensitivity to stress (Tavladoraki et al., 2012; Yamaguchi et al., 2006). Indeed, polyamines bind to ion channels and restrict the influx of sodium ions into roots, thus preventing the loss of potassium ions from shoot during stress (Zhao et al., 2007). They also occur as conjugates with hydroxycinnamic acids (coumaroyl, caffeoyl, feruloyl or sinapoyl derivatives), which have been suggested to be implicated in the protection against pathogens.

In plants, the most abundant polyamines are Put, Spd and Spm. Put is synthesized either from ornithine (Orn) by the Orn decarboxylase (ODC; EC 4.1.1.17) or from agmatine (Agm) via agmatinase (EC 3.5.3.12) using arginine as a precursor. The conversion of arginine to agmatine is catalyzed by the chloroplastic arginine decarboxylase (ADC; EC 4.1.1.19) whereas Orn is synthesized either from glutamate via several acetylated intermediates in chloroplasts or from arginine (Winter et al., 2015). Spd and Spm are synthesized from Put by the sequential addition of aminopropyl moieties via Spd/Spm synthases using decarboxylated *S*-adenosyl-methionine. Uncommon polyamines such as norspermidine (nSpd) and norspermine (nSpm) are present in plants (Hamana & Matsuzaki, 1985). Their catabolism including acetyl-derivatives involves copper-containing diamine oxidases and FAD-containing polyamine oxidases (PAOs, Bolkenius & Seiler, 1981; Federico et al., 1996; Landry & Sternglanz, 2003; Mamont et al., 1981), and the resulting *N*-acetyl-3-aminopropanal is oxidized further by aminoaldehyde dehydrogenases (ALDH10) (Kopečný et al., 2013).

Interestingly, the amino acids Orn and lysine (Lys), along with acetylated derivatives N^5-acOrn and N^6-acLys, accumulate under salt stress as a function of salt concentration, among primitive organisms such as halophilic bacterial strains *Bacillus aquimaris* VITP4 and *Planococcus maritimus* VITP21 (Joghee & Jayaraman, 2014). Lys is linked to abiotic and biotic stress responses (Batista-Silva et al., 2019; Kiyota et al., 2015).

Figure 1 shows examples of polyamine and amino acid acetylation. When Spm and Spd become acetylated, they no longer interact with RNA (Kakegawa et al., 1991). Polyamine acetylation via mammalian spermidine/spermine N^1-acetyltransferases (SSATs) promotes cellular export, with N^1-acSpd and N^1-acSpm being the major polyamines exported; for example, via the SLC3A2 transporter (Uemura et al., 2008). N^1-acSpm, N^1-acSpd, N^8-acSpd and acPut have been found in extracts of several plant species (Hennion et al., 2012). In Arabidopsis, a gene responsible for acetylation named *N-ACETYLTRANSFERASE ACTIVITY* codes for a SSAT1 (or NATA1, EC 2.3.1.57) (Adio et al., 2011; Lou et al., 2016). Accumulation of acPut and N^5-acOrn was observed upon hormonal treatment using methyl jasmonate (MeJA), which is known to induce plant defense responses. Very recently, a second enzyme denoted NATA2 was characterized in *Arabidopsis thaliana* (Mattioli et al., 2022).

SSATs belong to the superfamily called 'General Control Non-repressible 5- related *N*-acetyltransferase' (GNAT,

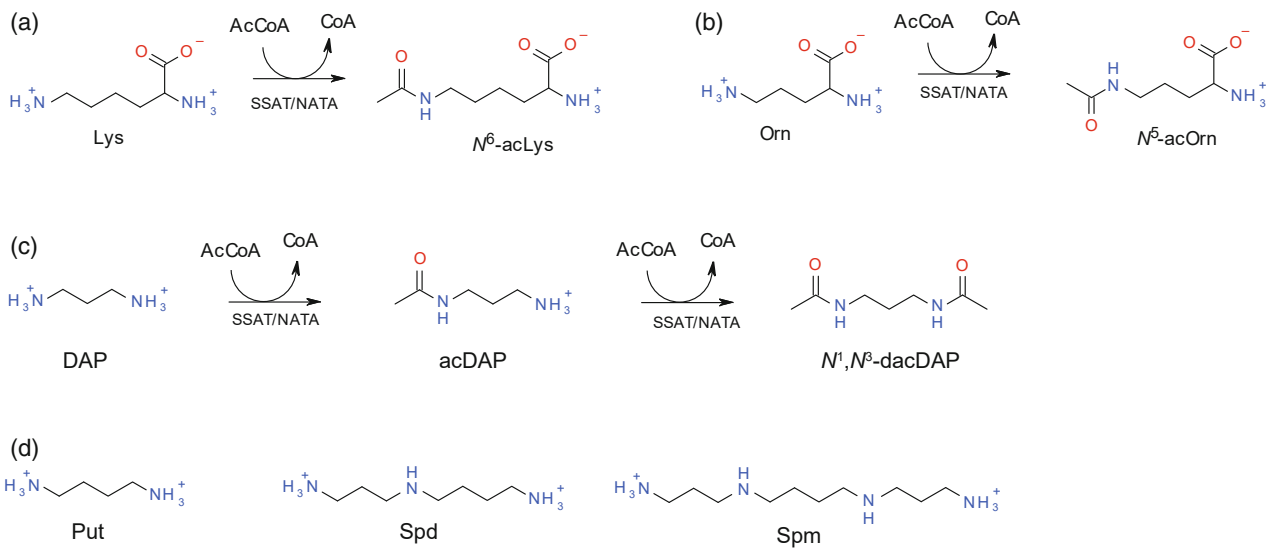

Figure 1. Reaction scheme of amino acid/polyamine acetylation via SSAT enzymes.
(a) Lys acetylation at N^6 atom.
(b) Orn acetylation at N^5 atom.
(c) DAP acetylation via monoacetylated derivative at N^1 atom; acCoA stands for acetyl-CoA.
(d) Structures of the other important polyamine substrates such as Put, Spd and Spm.

Neuwald & Landsnan, 1997) and catalyze the transfer of an acetyl group from an acetyl-CoA (acCoA) to an amino group of a broad range of substrates. GNAT members display low sequence identity but share the characteristic conserved core fold consisting of six to seven β-strands and four α-helices. So far, the crystal structures of the dimeric human SSAT1 (hSSAT1) and SSAT2 (hSSAT2) (Bewley et al., 2006; Han et al., 2006; Hegde et al., 2007; Zhu et al., 2006), the mouse enzyme (mSSAT1) (Montemayor & Hoffman, 2008) and the *Bacillus subtilis* SSAT (PaiA, Forouhar et al., 2005) are available. The hSSAT1 prefers longer polyamines over Put or Lys (Della Ragione & Pegg, 1983; Montemayor & Hoffman, 2008) in contrast to hSSAT2, which acetylates thialysine (thiaLys) and Lys (Coleman et al., 2004). *Bacillus subtilis* SSAT preferentially acetylates Spm, Spd and nSpd. The bi-substrate complex of hSSAT1 with N^1-Spm-acCoA and kinetic experiments revealed that the enzyme catalyzes an acid/base-assisted reaction and follows a suggested random sequential mechanism. Tyr140 acts as a general acid, whereas Glu92 serves as a general base to perform water-mediated deprotonation of the polyamine substrate (Hegde et al., 2007). The E92Q mutant of mSSAT confirmed the essential role of Glu92 in the reaction (Montemayor & Hoffman, 2008).

In the present study, we investigated three SSAT/NATA enzymes from two distantly-related plant species: one SSAT from moss (*Physcomitrium patens*) and two from the monocot maize (*Zea mays*). The unique single-exon *PpSSAT* gene (Phytozome ID: Pp3c5_21790V3.1) encodes a 214 amino acids long protein. The maize genome comprises two *SSAT* genes *ZmSSAT1* (AC149475.2_FGT007) and *ZmSSAT2* (AC209858.4_FGT004) coding for 225 and 227 amino acids proteins, respectively, and sharing 92% sequence identity. PpSSAT shares 29% sequence identity with hSSAT1 and hSSAT2 versus 45% and 48% identity with monocot orthologues from maize and the dicot orthologues from Arabidopsis (AtNATA1 and AtNATA2), respectively (Table S1). Until now, no experimental structure of plant SSAT/NATA was available and the substrate specificity for AtNATA1 reported in the literature was conflicting. Indeed, the preferred substrates were Orn (Adio et al., 2011), then 1,3-diaminopropane (DAP) with thiaLys (Jammes et al., 2014) and later Put (Lou et al., 2016). We focused on the kinetics of the three above plant SSATs and solved two high-resolution crystal structures of moss SSAT ternary complexes [acCoA with a polyethylene glycol (PEG) mimicking Spm, and CoA with Lys]. The role of key residues affecting the substrate specificity was characterized using site-directed mutagenesis and affinity measurements by microscale thermophoresis. Levels of free and acetylated polyamines and amino acids were measured in maize and moss samples to identify the most abundant acetyl derivatives under normal conditions and for moss also under various abiotic stresses.

RESULTS

Moss and maize SSATs exhibit broad substrate specificity

First of all, the molecular properties of all three plant SSATs were analyzed to optimize buffer composition for storage and kinetic studies (Figure S1). All three enzymes form dimers in solution as measured by size-exclusion chromatography with molecular masses between 50 and 52 kDa. The molecular weight of their monomers including the *N*-terminal His-tag ranged between 26.1 and 27.1 kDa. We further studied the effect of pH and buffer composition on thermal stability via nano-differential scanning fluorimetry and turbidity measurements. In general, basic pH decreased stability, whereas pH 7.0 led to the highest melting temperatures (data not shown). Both putative substrates and coenzymes also affected the thermal stability and aggregation of plant SSATs (Figure S1). For PpSSAT, Lys and Orn showed a modest positive effect on protein stability, whereas Spd and Spm displayed a modest negative effect leading to the earlier onset of aggregation. The presence of coenzyme stabilized the enzyme and acCoA displayed a stronger effect than the malonyl-CoA. The presence of the coenzyme also delayed the onset of aggregation. Both ZmSSATs behaved alike and were stabilized by the coenzyme. However, the effect of putative substrates on stability was only negligible compared with PpSSAT.

In the second step, aliphatic diamines such as DAP, Put, cadaverine, Agm, polyamines including nSpd, Spd, nSpm, Spm, as well as amino acids (Lys, Orn, L-citrulline) and several aromatic amines (2-phenylethylamine, tyramine and histamine), were screened as potential substrates of the three SSATs using a fixed 0.5 mM concentration of the acCoA coenzyme (Table 1). PpSSAT activity with 5 mM DAP was 1.1 nmol sec^{-1} mg^{-1}, whereas the activities of ZmSSAT1 and ZmSSAT2 were five to six times higher, respectively, reaching 5.4 and 6.5 nmol sec^{-1} mg^{-1}. PpSSAT displayed the highest rate for DAP, and 20–30% acetylation for Spm, nSpm and Lys compared with DAP (Figure 2a). Both ZmSSATs showed very similar activity, as expected from their high sequence identity. They acetylated Lys slightly faster than DAP (approximately 95% compared with Lys, Figure 2a), whereas the conversion of all the other di-/polyamines was slower. For all enzymes, nSpm and nSpd were acetylated at a similar rate as Spm and Spd, respectively. Aromatic amines especially histamine can serve as substrates. Finally, Put as well as Orn were very poor substrates (< 10% rate versus the preferred substrate) although their acetyl metabolites were reported from previous studies in various organisms as putative products of the SSAT/NATA reaction. Our HPLC-MS analysis revealed that neither Lys, nor Orn was acetylated at the N^{α} amino group, thus producing only N^6-acLys and N^5-acOrn (Figure S2).

Table 1 Substrate screening of plant SSAT/NATAs from moss and maize with various polyamines and amino acids

	Relative activity (%)		
Substrate	PpSSAT	ZmSSAT1	ZmSSAT2
Lys	20.5 ± 2.3	100.0 ± 2.0	100.0 ± 0.5
Orn	1.3 ± 0.3	5.0 ± 0.7	7.8 ± 2.4
DAP	100.0 ± 4.5	96.8 ± 1.8	90.0 ± 4.7
AcDAP	28.4 ± 3.1	38.2 ± 4.1	31.3 ± 4.4
Put	5.0 ± 0.8	8.0 ± 0.4	9.2 ± 0.3
Cadaverine	1.4 ± 5.2	2.1 ± 0.5	2.8 ± 0.4
Agm	2.8 ± 0.2	2.4 ± 0.3	3.1 ± 0.4
NSpd	16.8 ± 9.1	12.8 ± 2.2	12.8 ± 2.6
Spd	14.7 ± 1.3	9.3 ± 1.5	7.8 ± 2.8
N^8-AcSpd	8.5 ± 1.8	6.5 ± 1.5	5.6 ± 2.7
NSpm	24.6 ± 2.9	17.7 ± 3.3	13.6 ± 0.7
Spm	32.8 ± 2.2	14.7 ± 1.1	12.1 ± 1.3
N^1-AcSpm	12.4 ± 1.4	8.3 ± 0.5	6.4 ± 0.7
Citrulline	0.6 ± 0.4	0.3 ± 0.4	0.3 ± 0.4
2-Phenylethylamine	2.9 ± 0.1	1.6 ± 0.4	1.2 ± 0.2
Tyramine	0.7 ± 0.1	0.9 ± 0.1	0.5 ± 0.1
Histamine	8.0 ± 0.5	13.1 ± 1.8	10.1 ± 1.5

Measured in 100 mM Tris–HCl, pH 7.5, 0.5 mM acCoA with 5 mM substrates using a continuous DTNB assay at 30°C. Specific activity of PpSSAT was 1.1 nmol sec^{-1} mg^{-1}, that of ZmSSAT1 was 5.4 nmol sec^{-1} mg^{-1} and that of ZmSSAT2 was 6.5 nmol sec^{-1} mg^{-1} when measured with DAP.

Noteworthy, monoacetyl derivatives such as acDAP, N^8-acSpd or N^1-acSpm can also be acetylated to form diacetyl diamine products (not analyzed in the present study).

The three enzymes displayed the highest rates for a cytotoxic Lys antimetabolite, named thiaLys (*S*-aminoethyl-L-cysteine), so far identified in mammalian tissues (Cavallini et al., 1991; Jun et al., 2003). The relative activity of PpSSAT with thiaLys was 90-fold higher than with Lys and, for both ZmSSATs, the activity was approximately 12-fold higher than with Lys. The existence and the role of thiaLys in plants are questionable, and thus this compound was not studied further here. In the case of hSSAT2, the acetylation rate for thiaLys was reported to be five-fold higher than for Lys (Coleman et al., 2004).

The kinetic properties of the major substrates Spm, Spd, Put, DAP, Orn and Lys identified above were examined in detail for PpSSAT and one ZmSSAT because ZmSSAT1 and ZmSSAT2 display similar activities (Table 2; Figure 2a). A comparison of the catalytic efficiency values (V_{max}/K_m) indicated that the best substrate of PpSSAT and ZmSSAT2 was Spm and Lys, respectively, followed by DAP for both. ZmSSAT1 and ZmSSAT2 displayed similar kinetic values for Lys: K_m of 6.8/6.1 mM and V_{max} of 14.1/16.7 nmol sec^{-1} mg^{-1}, respectively.

Moss and maize SSATs display a strong affinity for AcCoA

The tested SSATs displayed a K_m value of approximately 60–75 μM for acCoA coenzyme (Table 2; Figure S3). The second tested coenzyme was malonyl-CoA, which is one carbon longer and negatively charged. The studied SSATs can bind malonyl-CoA and malonylate DAP, at lower rates and significantly higher K_m values compared with DAP acetylation. Relative catalytic efficiency (V_{max}/K_m) with malonyl-CoA was below 11% compared with acCoA for all tested enzymes.

Binding affinities (K_D values) for acCoA and malonyl-CoA were further measured by microscale thermophoresis (MST) (Table 3) and they were similar to K_m values. PpSSAT displayed a unique combination of negative thermophoretic curves (negative Soret effect) in the absence of ligand and positive thermophoretic curves upon ligand binding (positive Soret effect), providing a large normalized difference of the fluorescence signal and thus high sensitivity to test the binding of various ligands (Figure S3). For PpSSAT, the K_D values of 47 ± 4 μM for acCoA (coenzyme substrate) and 51 ± 3 μM for CoA (coenzyme product) were five times lower than for malonyl-CoA. A similar pattern was observed for ZmSSAT1 (and ZmSSAT2) having K_D of 13 ± 2 μM (21 ± 6 μM) for acCoA and 38 ± 3 μM (52 ± 18 μM) for malonyl-CoA, respectively.

Substrate affinities for PpSSAT can change in the absence or presence of coenzyme

Next, we focused on PpSSAT and measured substrate affinities for the apoform only and for the PpSSAT–CoA complex (coenzyme product) (Table 3) to identify whether the coenzyme has an impact on substrate binding. In the absence of coenzyme, the binding of Lys and Orn differs from di- and polyamines. Indeed, Lys and Orn (K_D in the low millimolar range) bind stronger than polyamines (especially Spd and DAP) and their K_D values are similar to their K_m values. The affinity for thiaLys (2.6 ± 0.4 mM) was almost identical to that for Lys (2.2 ± 0.3 mM) as shown with PpSSAT. By contrast, K_D values for the long polyamines Spm and Spd are much higher than their K_m values, suggesting that acCoA contributes positively to their binding (Figure S4). This was confirmed by adding 1 mM CoA and measuring the binding with the PpSSAT-CoA complex. Indeed, this time, K_D values for the di- and polyamines were much lower and similar to K_m values. By contrast, the presence of CoA did not change any affinity towards amino acids Lys and Orn (Figure 2b; Table 3).

The inhibitory properties of amino acids lacking α-amino group such as β-alanine (β-ALA), γ-aminobutyric acid (GABA) and trimethyl-γ-aminobutyric acid (TMABA), thus mimicking the bound substrate, were tested (Figure S4). β-ALA and GABA are not acetylated as verified by HPLC, and TMABA cannot be an SSAT substrate as a result of of its methylated nitrogen. Remarkably, these three compounds inhibit the acetylation of Lys but not that of DAP in PpSSAT. TMABA displays the highest affinity

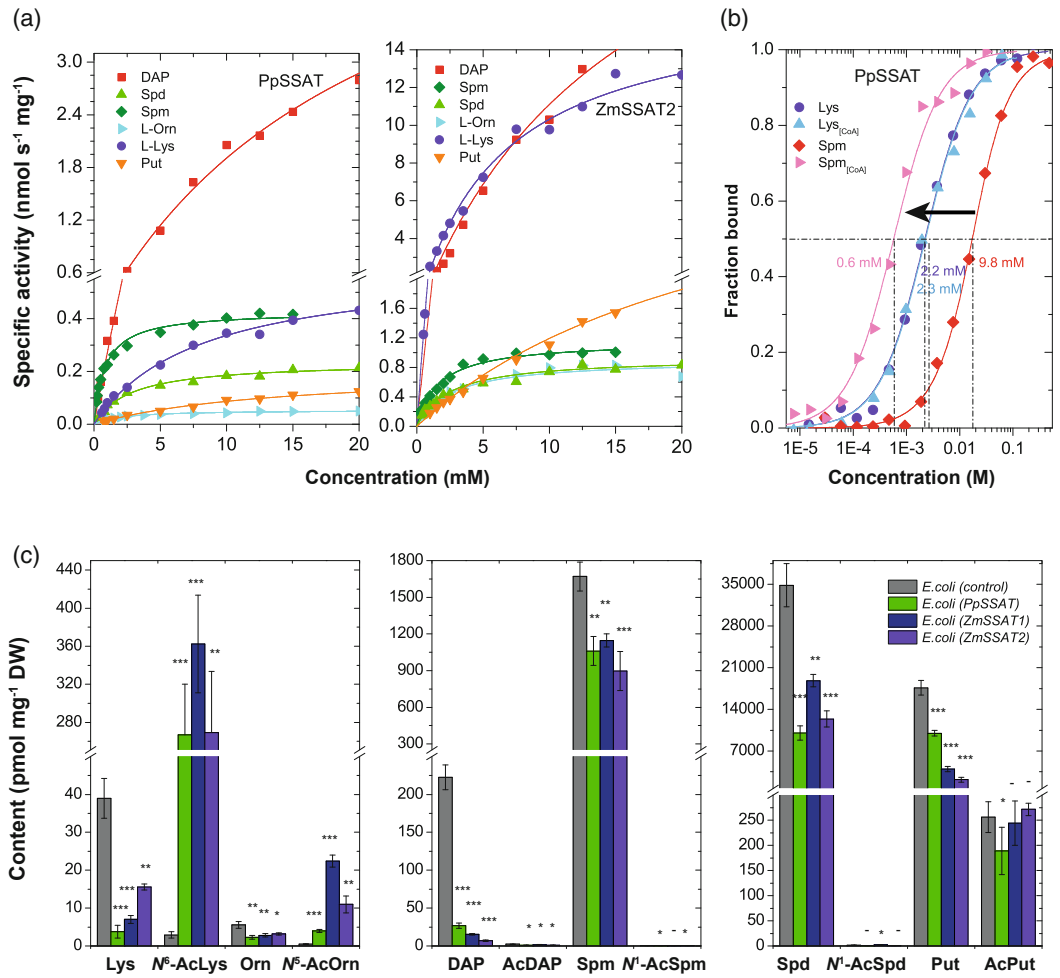

Figure 2. Enzyme kinetics of two plant SSATs towards substrates and *in vivo* altered metabolites in *E. coli* strains.
(a) Saturation curves of PpSSAT and ZmSSAT2 measured at saturating 0.5 mM concentration of acCoA in 100 mM Tris–HCl, pH 7.5.
(b) Example of binding affinity change of PpSSAT for substrates in the presence of the apoform only (binary complex) or in the presence of the enzyme plus 1 mM CoA (ternary complex). The affinities were measured by MST in PBS buffer pH 7.0 with 0.05% Tween.
(c) Decreased levels of free Lys and Orn and accumulation of their acetylated derivatives, and decreased levels of DAP, Spm, Spd and Put in *E. coli* extracts upon expression of three plant *SSAT* genes in pET28b vector at 20°C overnight. Asterisks indicate significant differences between the control and the overexpressor lines at $*P < 0.05$, $**P < 0.01$ and $***P < 0.001$, according to Student's *t*-test.

(K_D of 1.6 mM) measured by MST, and inhibits the acetylation of 1 mM Lys the most effectively (by approximately 50% using 10 mM TMABA).

Polyamines and amino acids are substrates of plant SSATs expressed in *Escherichia coli*

The SSAT major substrates were confirmed *in vivo* upon analyzing extracts of *E. coli* overexpressing *PpSSAT* and *ZmSSAT1/2* (Figure 2c). Levels of free Lys and Orn decreased and their acetyl products N^6-acLys and N^5-acOrn accumulated compared with *E. coli* control cells carrying an empty vector. Similarly, levels of polyamines Spm and Spd, which were the highest in bacteria, as well as Put and DAP, decreased. Nonetheless, the accumulation of their acetylated derivatives was not observed.

Gene expression and polyamine/amino acid levels in moss and maize

The effect of abiotic stress responses on moss *SSAT* gene expression was analyzed in liquid Knop under various stresses comprising high salinity, drought, low and high nitrogen content (10/200% of nitrate), as well as hormone treatments with either MeJA, ABA or cytokinin benzyl adenine. It can be summarized that *PpSSAT* expression is very robust and constitutive under various abiotic stresses because transcript levels remained almost unchanged regardless of the treatment (Figure S5); a negligible increase was observed for sorbitol, MeJA and low nitrogen treatments.

Spd and Put were the most abundant [approximately 300–400 pmol mg^{-1} of dry weight (DW)] in liquid moss

Table 2 Kinetic parameters for substrates and coenzymes of SSATs from moss and maize

	PpSSAT			ZmSSAT2		
Ligand	K_m (mM)	V_{max} (nmol sec^{-1} mg^{-1})	V_{max}/K_m (relative)	K_m (mM)	V_{max} (nmol sec^{-1} mg^{-1})	V_{max}/K_m (relative)
Spm	0.8 ± 0.1[a]	0.43 ± 0.01[a]	100	1.7 ± 0.1[a]	1.2 ± 0.1[a]	26
Spd	3.1 ± 0.2[a]	0.24 ± 0.01[a]	15	2.5 ± 0.2[a]	0.91 ± 0.03[a]	13
Put	13.7 ± 8.2[a]	0.20 ± 0.01[a]	3	25.3 ± 2.0[a]	4.2 ± 0.2[a]	6
DAP	20.6 ± 1.5[a]	5.8 ± 0.2[a]	52	15.9 ± 0.9[a]	28.8 ± 0.6[a]	66
Lys	8.0 ± 0.8	0.61 ± 0.03	14	6.1 ± 0.5	16.7 ± 0.4	100
Orn	2.4 ± 0.2	0.06 ± 0.01	5	2.6 ± 0.3	0.93 ± 0.04	13
AcCoA	0.072 ± 0.005	6.0 ± 0.1	100	0.061 ± 0.003	27.1 ± 0.5	100
Malonyl-CoA	0.264 ± 0.029	2.3 ± 0.1	11	0.186 ± 0.017	3.7 ± 0.1	5

Saturation curves for the selected substrates were measured in 100 mM Tris–HCl, pH 7.5, and using saturating 1 mM acCoA concentration in a DTNB assay at 30°C. Saturation curves for acCoA and malonyl-CoA were measured at saturating 60 mM concentration of DAP. Kinetic constants K_m and V_{max} including their SE values were determined using PRISM, version 8.0.
[a]Stands for apparent K_m and V_{max} values as a second step of acetylation cannot be excluded.

Table 3 Binding affinities of plant SSATs for coenzyme and substrates

	PpSSAT		ZmSSAT1	ZmSSAT2
Ligand	K_D (mM)	$K_{D\ [CoA]}$ (mM)	K_D (mM)	K_D (mM)
AcCoA	0.047 ± 0.004	-	0.013 ± 0.002	0.021 ± 0.006
Malonyl-CoA	0.265 ± 0.037	-	0.038 ± 0.003	0.052 ± 0.018
Spm	9.8 ± 1.2	0.6 ± 0.1	ND	ND
Spd	102 ± 5	7.2 ± 3.2	ND	ND
Put	6.1 ± 1.2	4.4 ± 1.3	ND	ND
DAP	68.5 ± 8.2	31.1 ± 2.8	ND	ND
Lys	2.2 ± 0.3	2.3 ± 0.2	ND	ND
ThiaLys	2.6 ± 0.4	2.2 ± 0.5	ND	ND
Orn	2.8 ± 0.4	2.5 ± 0.3	ND	ND

The K_D values were measured by MST in the presence of the apoform only (i.e. absence of acCoA) or in presence of the enzyme plus 1 mM CoA ($K_{D\ [CoA]}$) in PBS buffer pH 7.0 with 0.05% Tween on Monolith NT.115 in premium capillaries. ND, not determined.

cultures (Table 4, control), whereas levels of DAP and Spm were below 3 pmol mg^{-1} of DW. Orn and Lys were present up to approximately 5 pmol mg^{-1} of DW including their acetylated derivatives. Levels of acetyl diamines and polyamines were very low (acPut and N^1-acSpm) or below detection limit (acDAP, N^1-acSpd and N^1-acnSpd). By contrast, DAP and Put were the most abundant metabolites in 2-week-old maize plantlets, grown in liquid MS medium, in both leaves and roots (up to 3000 pmol mg^{-1} of DW), whereas their acetylated forms were extremely low except for acPut in roots (Table 4). Levels of the remaining polyamines were below approximately 20 pmol mg^{-1} of DW and those of N^1-acSpd, N^1-acnSpd and N^1-acSpm were either negligible or below the detection limit, most likely as a result of either a low level of free precursors Spm, Spd and nSpd or high PAO activity. Indeed, it is well known that acetyl polyamines are good substrates of plant PAOs (Ahou et al., 2014; Federico et al., 1996; Kim et al., 2014). A high DAP amount likely indicates high PAO activity in maize. The most abundant acetylated derivative was N^5-acOrn at approximately 50 pmol mg^{-1} of DW. Although the export of amino acids is mediated by plant-specific UmamiT transporters (Müller et al., 2015), it remains elusive whether some of the UmamiT members can also export polyamines from cells or whether there is an unknown specific polyamine transporter. Finally, under stresses tested with moss, several differences in precursor levels were observed. Cultures exposed to sorbitol, MeJA or ABA contained the double amount of Orn and Put indicating a change in polyamine synthesis. However, nearly no change was observed for any acetylated derivative in line with the almost steady expression of the *PpSSAT* gene under all tested stresses (Figure S5).

Polyamine binding mode: crystal structure of PpSSAT in complex with acCoA and PEG

The co-crystal structure of PpSSAT with 5 mM acCoA was determined by molecular replacement using hSSAT2 [Protein Data Bank (PDB) 2BEI] as a search model (Han et al., 2006). The final model corresponds to a dimer present in the asymmetric unit. PpSSAT, hSSAT1 and hSSAT2 share the same topology and dimeric interface.

Table 4 Levels of selected polyamines and amino acids in moss and maize

	Levels of polyamines and amino acids (pmol mg^{-1} DW)						
	Moss (*Physcomitrium patens*)					Maize	
Metabolite	Control	NaCl	Sorbitol	MeJA	ABA	Leaves	Roots
Lys	4.4 ± 0.6	11.5 ± 7.0	4.6 ± 1.2	4.8 ± 0.8	5.4 ± 0.8	10.2 ± 1.8	34.7 ± 0.9
N^6-AcLys	4.1 ± 1.4	1.4 ± 0.1	1.9 ± 0.3	2.8 ± 0.6	1.2 ± 0.1	1.7 ± 0.21	1.8 ± 0.1
Orn	5.4 ± 1.5	13.6 ± 3.3	9.4 ± 1.4	8.7 ± 2.4	10.4 ± 1.2	1.5 ± 0.4	5.9 ± 0.4
N^5-AcOrn	2.9 ± 1.1	1.1 ± 0.2	3.70 ± 0.4	2.43 ± 0.3	1.94 ± 0.2	47.3 ± 6.8	41.5 ± 1.3
DAP	1.6 ± 0.6	13.8 ± 4.7	51.62 ± 9.7	1.58 ± 0.8	14.9 ± 2.4	2022.7 ± 257.9	2957.8 ± 242.2
AcDAP	ND	ND	ND	ND	ND	0.13 ± 0.01	0.19 ± 0.02
Put	296.1 ± 63.5	380.6 ± 243.3	664.8 ± 184.4	647.7 ± 37.9	755.1 ± 97.1	1938.9 ± 221.5	2328.7 ± 83.8
AcPut	0.27 ± 0.1	0.26 ± 0.1	0.27 ± 0.1	0.18 ± 0.02	0.16 ± 0.03	0.33 ± 0.04	2.19 ± 0.27
nSpd	8.2 ± 1.3	15.7 ± 3.2	20.2 ± 2.2	15.9 ± 3.6	17.5 ± 1.6	1.51 ± 0.21	1.49 ± 0.09
N^1-AcnSpd	ND	ND	ND	ND	ND	0.05 ± 0.01	0.16 ± 0.06
Spd	364.4 ± 107.0	434.3 ± 177.4	298.8 ± 59.6	388.6 ± 57.8	427.0 ± 53.2	5.1 ± 0.99	20.9 ± 4.5
N^1-AcSpd	ND	ND	ND	ND	ND	ND	0.04 ± 0.01
Spm	2.7 ± 1.6	4.7 ± 2.0	4.9 ± 1.0	2.2 ± 0.7	9.6 ± 1.7	3.7 ± 0.6	5.7 ± 1.4
N^1-AcSpm	0.31 ± 0.04	0.25 ± 0.03	0.38 ± 0.3	0.41 ± 0.09	0.24 ± 0.01	ND	ND

MS data represent the average values (n = 3) with SD of moss grown in a liquid Knop medium supplemented with either 200 mM NaCl or 400 mM sorbitol or treated with 10 μM ABA or MeJA for 4 days. Maize was grown in standard MS medium. ND, not detected.

Superposition of PpSSAT and hSSAT1 dimers (PDB 2F5I) gives an RMSD of 1.56 Å for 311 Cα atoms, whereas that with hSSAT2 gives an RMSD of 1.93 Å for 300 Cα atoms. Plant enzymes contain an additional approximately 40 amino acids long segment (Mattioli et al., 2022), from position 68 to 114 in PpSSAT numbering, absent in mammalian SSATs (Figure S6). This segment inserted between the β2 and β3 strands (Figure 3a,b) comprises an extra β strand (named here as β3*), antiparallel to the β1 strand, making the central β sheet larger. This extra β3* strand is located near the coenzyme site, namely the P-loop, which is composed of six amino acids Arg-X-X-Gly-X-Gly (Lu et al., 1996) interacting with the adenosine part of acCoA via water molecules.

Both monomers of PpSSAT are very similar as indicated by the RMSD of 0.80 Å for 197 Cα atoms. Nonetheless, a large movement is observed in the region 188–193 containing the α4 helix (residues 181–188) (Figure 3c), which delineates the coenzyme cleft together with the α3 helix. Each subunit binds acCoA in a different conformation except for the pyrophosphate group, which makes identical interactions with the backbone of the conserved residues Arg149, Gly152 and Gly154 from the P-loop plus one side chain contact with Thr155. Residues making hydrophobic and polar interactions with the whole acCoA coenzyme are listed in Figure 3d (details of used sequences are in Table S3). In subunit A, the adenosine 3′-phosphate moiety from the coenzyme is poorly defined in electron density maps (Figure S7) and adopts an extended conformation without protein interaction. This allows Asn181 and Tyr188 side chains from the α4 helix to interact with the pantothenate moiety of the cofactor. In subunit B, the whole acCoA, which is very well defined in electron density maps (Figure S7), adopts a 'compact form' with the adenine moiety rotated by 180° compared with subunit A (Figure 3e–g).

The compact conformation of acCoA appears due to the presence of a PEG molecule (1PE), originating from the crystallization conditions, which is bound in the substrate binding site in subunit B (Figure 4a) but absent in subunit A (Figure 4b). This molecule mimics the Spm substrate and forms a ternary complex. Bound PEG molecule pushes the acetyl moiety of the cofactor, which in turn pushes the side chain of Tyr188 and thus the whole α4 helix upwards by approximately 3 Å, leaving space for the adenosine moiety of coenzyme and allowing it to adopt the compact conformation (Figure 4c). The adenine is thus stacked on the aromatic side chain of Phe187 and is hydrogen (H)-bonded to the Tyr188 side chain as well as to Asn181 and Asn183 via water molecules. The same compact form of acCoA was reported in the crystal structure of hSSAT1 in complex with the bisubstrate analog/inhibitor, N^1-Spm-acCoA (Figure 4d), mimicking both the bound Spm and acCoA (PDB 2JEV, Hegde et al., 2007). The conformation is different from that observed with only the coenzyme bound (PDB 2B3V; Bewley et al., 2006).

We were able to model a bent pentaethylene glycol ligand (1PE) into the continuous electron density map in the active site of subunit B (Figure S7). It mimics Spm substrate, slightly shorter than 1PE, and creates a groove by opening the substrate-binding site, not observable in the empty subunit A (Figure 4a,b). It establishes numerous H-bond interactions directly or through water molecules with several residues including Glu140, Cys176 and Tyr138,

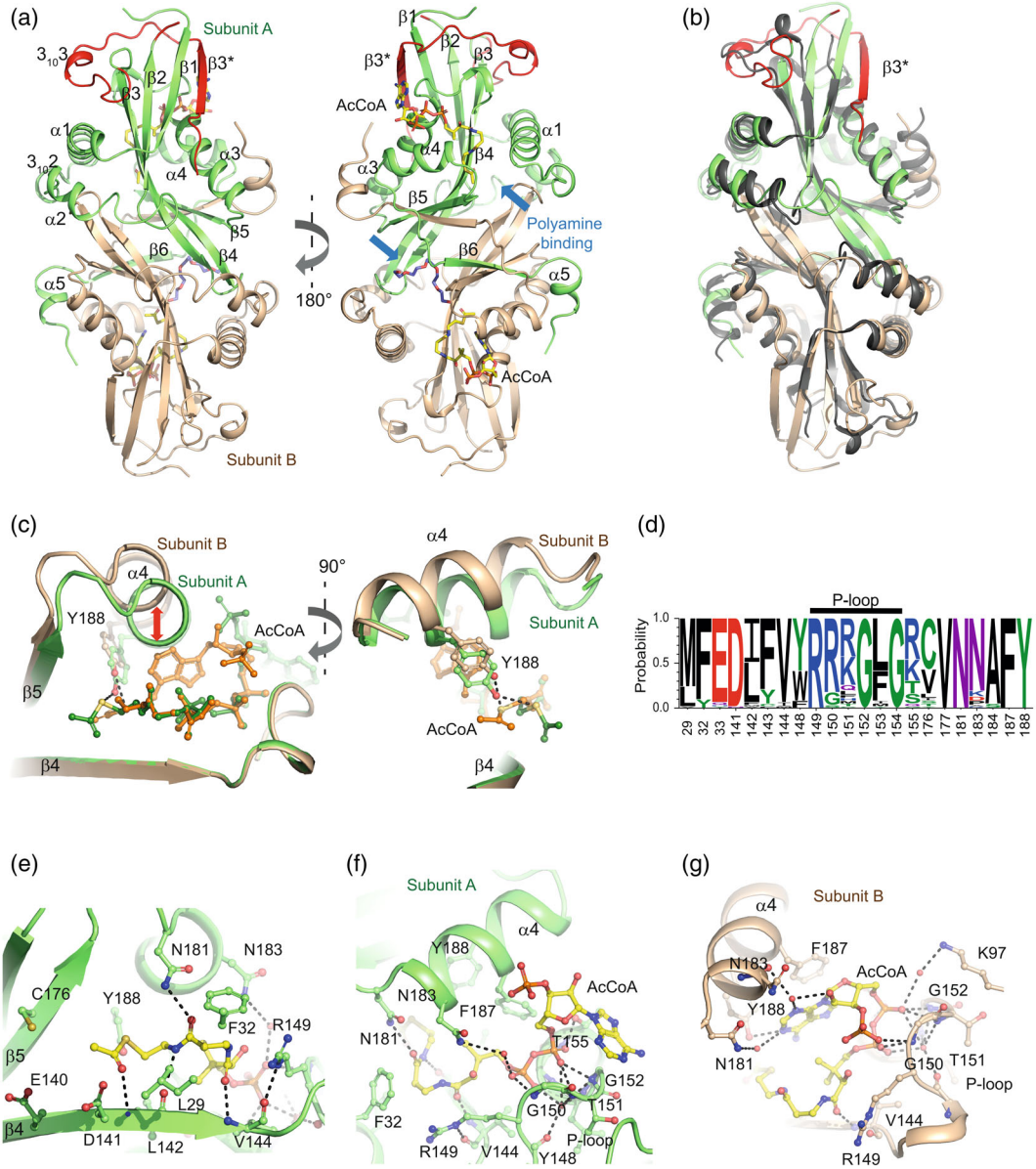

Figure 3. Quaternary structure of PpSSAT and binding of acCoA.
(a) Two views of the ribbon representation of the PpSSAT dimer including its topology description. Subunits A and B are colored green and light brown, respectively. Ligands are shown as sticks, the acCoA is in yellow and the polyethylene molecule (1PE) bound to the active site of the subunit B is in violet. The additional segment found only in plant SSATs is colored in red in subunit A.
(b) Superposition of PpSSAT (present study, PDB 7ZHC) with SSAT1 from *H. sapiens* (PDB 2JEV). SSAT1 and PpSSAT are colored in gray and green–brown, respectively.
(c) The binding site superposition of PpSSAT subunits reveals a movement of the α4 helix in the vicinity of acCoA, which is shown in green and brown color in subunits A and B, respectively. Tyr188 residue is labeled.
(d) Conservation of residues forming the coenzyme-binding site as deduced from 60 plant SSAT sequences. The numbering follows the PpSSAT sequence. The sequence logo was made using WEBLOGO 3 (http://weblogo.threeplusone.com).
(e) A close-up view of the β-mercaptoethylamine and pantothenate groups of acCoA in the subunit A.
(f, g) Binding site of acCoA (yellow) and interactions shown in black dashed lines between the coenzyme and the subunit A (green) and the subunit B (light brown).

which are key residues located deeper in the active site (Figure 4e,f). The role of Glu140 and C176 was investigated by site-directed mutagenesis (Table 5; Figure S8). The E140A mutation weakens the affinity to Spm (disruption of the water network) and reduces the specific activity by one order of magnitude (Table 5). The Cys176 affects both polyamine binding as well as the acetylation rate. Its side chain is H-bonded to Tyr138. Both residues would

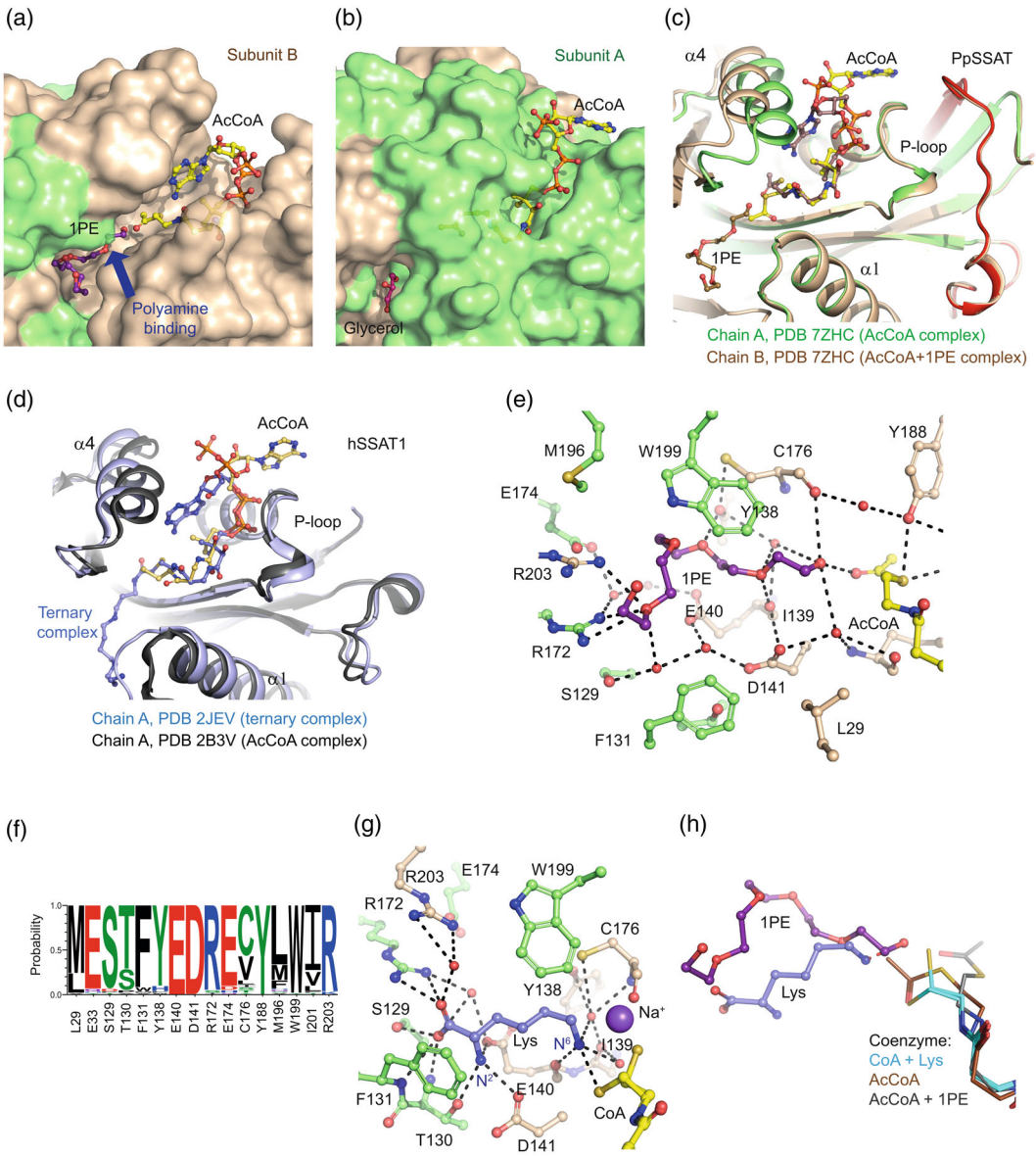

Figure 4. The active site of the ternary PpSSAT complexes.
(a) The open polyamine-binding site with bound polyethylene glycol (PEG is shown in violet) in subunit B (light brown), subunit A is in green and acCoA in yellow.
(b) The closed polyamine-binding site in the absence of polyamine in subunit A (green). A glycerol molecule (in magenta) is located at the groove entrance and acCoA is shown in yellow.
(c) The superposition of chains A and B in PpSSAT shows the α4 helix movement in a complex with acCoA + 1PE mimicking Spm (subunit colored in brown).
(d) The superposition of chains A of two hSSAT1 structures reveals the α4 helix movement in the complex with the bi-substrate analog (in blue, PDB 2JEV). The complex with only acCoA is shown in black (PDB 2B3V).
(e) Interactions of bound PEG molecule (colored in violet) mimicking Spm in the active site of PpSSAT (subunit A and B residues are in green and in light brown, respectively). AcCoA is in yellow.
(f) Conservation of the interacting active-site residues among plant SSATs.
(g) Interactions shown in black dashed lines of the bound Lys (in blue) with the enzyme. AcCoA is in yellow.
(h) Superposition of the subunits containing the bound Lys and PEG molecule (1PE).

establish water-mediated bonds with the N^1 and N^4 atoms of Spm (Figure S9), as manually modeled based on the 1PE molecule. Designed C176A and C176V mutations disrupt the water-mediated interactions and the resulting variants displayed 10-fold lower specific activities with Spm (Table 5) and three- to four-fold lower affinity for Spm than in wild-type (WT). Among the tested poly-/diamines, the C176A/V mutants displayed three times

Table 5 Substrate screening of active-site variants of PpSSAT

Enzyme	Spm activity (nmol sec^{-1} mg^{-1})	Relative rate (%)						Affinity K_D (mM)	
		Spm	Spd	Put	DAP	Lys	Orn	Spm	Lys
WT	0.392	100 ± 6	51 ± 2	13 ± 3	285 ± 13	66 ± 7	4.5 ± 0.5	9.8 ± 1.2	2.2 ± 0.3
E140A	0.024	100 ± 3	66 ± 7	28 ± 6	92 ± 7	26 ± 6	7 ± 1	41.4 ± 6.6	33.6 ± 4.1
C176A	0.024	100 ± 5	52 ± 8	18 ± 4	580 ± 52	330 ± 10	49 ± 9	37.8 ± 4.3	2.8 ± 0.4
C176V	0.028	100 ± 7	57 ± 11	42 ± 5	460 ± 40	270 ± 4	35 ± 8	29.8 ± 7.1	9.6 ± 1.1
R172A	0.472	100 ± 4	34 ± 3	12 ± 2	229 ± 21	18 ± 6	2 ± 0.2	11.4 ± 3.3	15.6 ± 2.2
R203A	0.432	100 ± 2	58 ± 8	8 ± 2	165 ± 5	6 ± 1	2 ± 0.5	60.1 ± 8.3	25.3 ± 4.3
M196A	0.352	100 ± 9	70 ± 7	25 ± 3	184 ± 11	21 ± 5	11 ± 6	45.0 ± 5.6	25.2 ± 5.2

The specific activity of variants was measured in 100 mM Tris–HCl, pH 7.5, 1 mM acCoA with 5 mM Spm as the best substrate. Substrates preferences were screened with selected ligands as a relative rate to Spm using a continuous DTNB assay at 30°C. The affinity to Spm and Lys was measured by MST in PBS buffer with 0.05% Tween with 65 nM PpSSAT labeled with RED-tris-NTA second Generation His-Tag Labeling Kit.

faster relative acetylation rate for DAP versus Spm than in WT. The model of bound DAP is shown in Figure S9. Because water-mediated interactions comprise the terminal part of the coenzyme, a mild effect on the acCoA binding was observed as well. Although WT-PpSSAT displays a K_m value of 72 ± 5 μM and a K_D value of 47 ± 4 μM for acCoA, both C176V and C176A mutants display slightly lower K_m values of 41 ± 2 μM and 30 ± 3 μM, respectively, as well as a slight change in the affinities (K_D of 9 ± 2 μM and 17 ± 6 μM) (Figure S8).

Amino-acid binding mode: crystal structure of PpSSAT in complex with CoA and Lys

A ternary complex of PpSSAT with Lys and the CoA product was solved at 2.06 Å resolution (PDB 7ZKT) to describe the binding of amino acid. The asymmetric unit contains four similar dimers with each site occupied by a Lys substrate and a product CoA. The coenzyme product, which lacks the acetyl moiety, adopts the same conformation, as does the acCoA in the subunit A (empty active site) in the above-described structure (PDB 7ZHC). Bound in the form of a thiolate anion, its charge is compensated by a near sodium ion (Figure 4g), which is within a 3.5 Å-distance of the side chains of Glu33 and Asn181 and the main chain nitrogen of Leu178.

The Lys substrate interacts with several residues in the active site. Indeed, its carboxyl group makes a salt bridge with Arg172, direct H-bonds with the side chain of Ser129 and the main chain NH of Thr130 and Phe131, and an additional water-mediated H-bond with Arg203. Its N^{α} amino group (N^2 atom) interacts with the carboxylates of Glu140 and Asp141 and the side chain of Thr130. All these interactions prevent the N^6 amino group of Lys to protrude as deep as the N^1-atom of Spm (mimicked by the PEG molecule; Figure 4h) towards the acetyl moiety of the coenzyme. Two aromatic residues, namely Phe131 and Trp199 (Trp84 and Trp154 in hSSAT1), are conserved in all species and form the middle part of the substrate cavity. The N^6 amino group interacts with the thiolate anion of CoA, the main chain oxygen of Glu140 and two water molecules, which in turn interact with both the side chain and main chain nitrogen of Cys176, the side chain of Tyr138, and the main chain oxygen of Ile139. The role of Glu140, Cys176, Arg172 and Arg203 was investigated by site-directed mutagenesis (Table 5; Figure S8). The E140A mutation weakens the affinity to Lys via the N^2 amino group and reduces the specific activity by one order of magnitude (Table 5). Both R203A and R172A mutations did not alter the activity with Spm but reduced the acetylation rate of Lys by up to 10-fold compared with the WT. Both mutants display lower affinities to Lys (K_D values are seven- and 10-fold higher).

DISCUSSION

A different binding mode of polyamines versus lysine

The present study reports a systematic analysis of substrate preferences of plant SSATs from moss and maize, combining different technical approaches such as colorimetric activity determination using DTNB, verification of substrate conversion using MS, and affinity measurements using MST on numerous diamines, polyamines and amino acids. By contrast to the human SSATs, which are more specific either towards polyamines (hSSAT1) or thiaLys and Lys (hSSAT2), we showed that three plant SSATs display a broad specificity, allowing acetylation of all the tested substrates, even though, *in vitro*, PpSSAT is more active on DAP and ZmSSATs are more active on Lys. Based on kinetic parameters V_{max}/K_m, and not on activities, Spm is the preferred substrate for PpSSAT and Lys for ZmSSATs. We also showed that, without the coenzyme, PpSSAT binds Lys and Orn more strongly than polyamines. Remarkably, a bound coenzyme increases plant SSATs affinity for polyamines, approaching affinities towards amino acids, suggesting that the binding mode of these two types of substrates (amino acids versus polyamines) is slightly different. It is noteworthy that a bound

coenzyme did not modify the enzyme's affinity for amino acid substrates. Therefore, the carboxylate group of amino acids, which distinguishes them from polyamines, appears to play an essential role in their binding mode. Accordingly, Put, which is a decarboxylated Orn, displayed higher K_D values (i.e. worse affinity) than Orn.

The two high-resolution ternary structures of PpSSAT, one with Lys substrate and the product CoA and the other with a PEG molecule mimicking a bound polyamine substrate and acCoA, illustrate and highlight the two modes of substrate recognition. The carboxylate group of Lys is recognized by two positively charged Arg172 (direct interactions) and Arg203 (water-mediated interactions) which are conserved among plants (Figure 4g). The N^2 amino group of Lys is tightly held by the three side chains of Glu140, Asp141 and Thr130, preventing its terminal N^6 amino group to protrude as deep as the N^1-atom of Spm, mimicked by the PEG molecule (Figure 4e,h) towards the acetyl moiety of the coenzyme. This illustrates an absence of coenzyme contribution towards the binding of Lys and Orn as deduced from the similar K_D measured in the absence and presence of the coenzyme and K_m values. The substrate–coenzyme product structure may explain the slower acetylation rate of Orn versus Lys. Although the distance between the attacking N^6 amino group and the thiolate anion of CoA is approximately 3.0 Å, the N^5 amino group in Orn, which is shorter than Lys, would be approximately 1.1 Å further from the thiolate group. Although Lys and PEG (mimicking bound Spm) bind in the same cavity, they do not fully overlap (Figure 4h). Inhibition experiments further support the different polyamine binding mode because the amino acids TMABA, GABA or β-ALA can inhibit the acetylation of Lys but not that of the short diamine DAP (Figure S4).

The superposition of the active site of PpSSAT plus Lys with those of hSSAT1 and hSSAT2 clarifies various substrate preferences (Figure 5a). Although interactions with the N^2 amino group of Lys in hSSAT2 are identical to those on PpSSAT (Glu92, Asp93 and Thr83), in hSSAT1, the latter threonine residue is replaced by a sterically unfavorable proline (Pro83). The second major difference arises in the interaction with the carboxylate moiety of Lys, where the serine residue in PpSSAT (Ser129) and hSSAT2 (Ser82) is replaced by an aspartate residue (Asp82) in hSSAT1. The negatively charged aspartate repulses the carboxylate group of Lys and its presence explains why Lys or thiaLys were not reported among substrates for hSSAT1 (Coleman et al., 2004). The interaction with the carboxylate groups of amino acids in plant SSATs is further strengthened by two conserved arginine residues (Arg172 and Arg203) absent in human or other mammalian SSATs. In line with high active-site homology, K_m values for substrates of plant SSATs, as measured in the present study, are similar to those for hSSAT2 substrates including DAP, Put, Spd and Spm, which are all in the low millimolar range (Coleman et al., 2004). The K_m value for thiaLys was reported as 0.3 mM. By contrast, hSSAT1 displays much lower K_m values of 4 and 58 μM for Spm and Spd, respectively (McCloskey & Pegg, 2003). Also, the k_{cat} values are below 1 sec^{-1}, when calculated from V_{max} values, and they are comparable to those reported for hSSAT2 or AtNATA2 (Coleman et al., 2004; Mattioli et al., 2022).

Finally, the extra β3* strand and the loop in plant SSATs are located over the P-loop and occupy a volume near the coenzyme site, which is absent in human SSATs (Figure 5b,c). This segment does not alter the position of any neighboring secondary structure. It can prevent several conformations of adenosine phosphate moiety observed in other SSAT structures. However, one of the allowed coenzyme conformations is similar to that observed in PpSSAT (Figure 5d). Therefore, binding of the coenzyme is not affected: K_m values for acCoA of 3 μM (Lu et al., 1996) or 4 μM (Coleman et al., 1996) were reported with hSSAT1, whereas slightly higher K_m values between 60 and 75 μM were found here for three plant SSATs in line with values of 5–71 μM reported for plant AtNATA1 (Lou et al., 2016).

ZmSSAT models are nearly identical to the PpSSAT structure

ZmSSAT models were constructed using Alphafold2 and were almost identical to the PpSSAT structure (RMSD of 0.95/0.99 Å over 190 Cα atoms of ZmSSAT1/2). There are several non-conserved residues that might be responsible for slight activity variations between ZmSSATs and PpSSAT. In the substrate channel, Met196 in the vicinity of Arg203 for PpSSAT is substituted by Leu197 in ZmSSATs. M196A mutation in PpSSAT shows that, although this residue is not in direct interaction, it weakens the affinity for substrates (Table 5). Two more residues found near the acetyl moiety of acCoA, namely Met36 and Ile143 in ZmSSATs (Leu29 and Leu142 in PpSSAT), could be responsible for activity differences (Figure S9). Ile residue can sterically alter the movement of the acetyl moiety of the coenzyme, whereas Met36 can interact with a water molecule located below the coenzyme. Moreover, the two positively charged Arg151 and Arg156 side chains in ZmSSATs (Gly150 and Thr155 in PpSSAT) near the P-loop might interact with the adenosine-phosphate group of acCoA. Indeed, both ZmSSATs display a slightly better affinity for acCoA (Table 3).

Catalytic mechanism of SSATs and key active-site residues of plant SSATs

The reaction mechanism of SSATs involves a transient formation of a ternary complex between acCoA, an amine substrate and the enzyme. A kinetic study on hSSAT1 using the bi-substrate analog N^1-Spm-acCoA suggested a random binding mechanism (Hegde et al., 2007). The

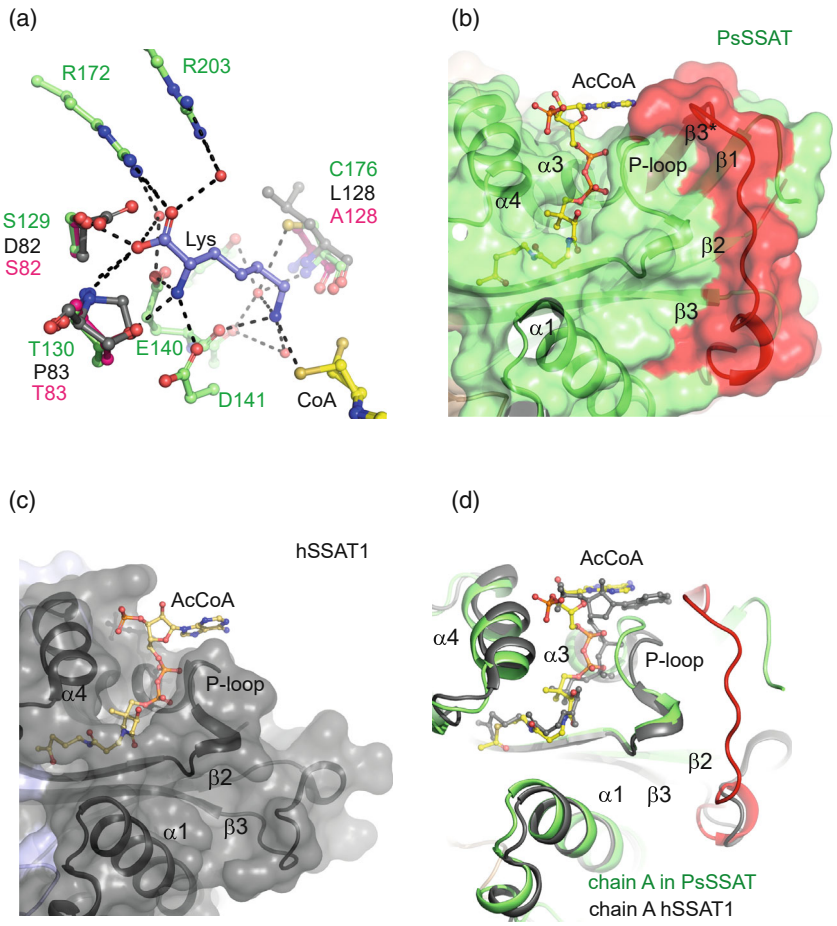

Figure 5. Mutual differences between plant and human SSAT.
(a) Three important differences in the active site linked to the interaction with Lys. PpSSAT is in green, hSSAT1 is in black and hSSAT2 is in pink.
(b) Detailed view at the extra approximately 40 amino acids long segment found among plant SSATs (in red) in PpSSAT located near the coenzyme site and the P-loop.
(c) Identical orientation of the coenzyme site, to that in (a), in hSSAT1 (PDB ID: 2B3V).
(d) Superposition of PpSSAT chain (green) and hSSAT1 chain (black) showing the position of the 40 amino acids long segment (in red) in the plant SSAT model.

random order is in line with our MST measurements showing that either substrate or coenzyme can bind in the absence of each other (Table 3). However, in the case of di- and polyamines, bound coenzyme increases the affinity for amine substrate as analyzed with PpSSAT (Figure 2b; Table 3). For example, the affinity for Spm (K_D of 9.8 mM) increases by more than 10-fold (K_D of 0.6 mM). This finding suggests that acetylation of especially longer amines may preferentially follow an ordered sequential mechanism, with the coenzyme bound in the first step. Accordingly, we were not able to crystallize PpSSAT with an amine substrate only, whereas we successfully cocrystallized the enzyme with acCoA only, resulting in a structure harboring the aliphatic 1PE molecule mimicking Spm only in subunit A, and not in subunit B. Moreover, Spm alone appears to induce aggregation of the enzyme, whereas the acCoA stabilizes plant SSATs (Figure S1).

The glutamate residue (Glu92 in SSAT1) was suggested to act as a general base and deprotonate an amine substrate, as well as a tetrahedral intermediate, via water molecules (Hegde et al., 2007; Montemayor & Hoffman, 2008). A general scheme suggests nucleophilic attack by the deprotonated amino group of the substrate on the carbonyl of the thioester generating a zwitterionic tetrahedral intermediate (Figure S10). Movement of the α4 helix as a result of PEG binding is similar to a large rearrangement observed for hSSAT1 in the presence of the transition state analog N^1-Spm-AcCoA (PDB 2JEV, Hegde et al., 2007) (Figure S7). The movement comprises a tyrosine residue (Tyr188 in PpSSAT, Tyr140 in hSSAT1), which interacts with the sulfur atom of acCoA. It was hypothesized to serve as a general acid that protonates the thiolate anion of CoA because its mutation to phenylalanine reduces the activity below 5% (Bewley et al., 2006; Hegde et al., 2007).

Here, we showed that the mutation of the equivalent Glu140 in PpSSAT significantly reduced the activity. However, the E140A mutant was not fully inactive, suggesting that this is not a unique general base. For example, two histidine residues were reported to assist the deprotonation step via water molecules in the serotonin *N*-acetyltransferase (Hickman et al., 1999; Scheibner et al., 2002). Analysis of the PpSSAT crystal structure indicates that the neighboring Glu33 and Asp141 may assist in amine substrate/ternary complex deprotonation. Indeed, the side chains of Glu140 and Asp141 bind a water molecule interacting with the substrate or directly the N^2 atom of the amino acid substrate (Figure 4e). All three negatively charged residues Glu140, Glu33 and Asp141 (Glu92, Glu28 and Asp93 in hSSAT1) are highly conserved in SSATs.

The fact that the thiaLys is acetylated much faster than Lys implies substrate-assisted catalysis. The electronegative sulfur atom lowers the pK_a value of the N^6 amino group by 0.49 (pK_a of N^6 amine is 10.29 in Lys and 9.82 in thiaLys). The calculated pK_a value of the same amino group in the tetrahedral intermediate is also lowered from 7.43 in the Lys-acCoA complex to 6.9 in the thiaLys-acCoA complex (Figure S10). Because the dissociation of the tetrahedral complex is accompanied by the loss of charge, the lower pK_a is in line with faster deprotonation and dissociation into the acetyl-thiaLys product and CoA. Surrounding residues can further affect the pK_a values, although these complex interactions are hard to predict. In the present study, all three plant SSATs display much higher thiaLys activity than for Lys. High thiaLys activity was reported for hSSAT2 (Coleman et al., 2004), as well as for both SSATs (NATAs) from *A. thaliana* (Jammes et al., 2014; Mattioli et al., 2022) but not for Lys.

The polyamine molecule can adopt various conformations: a linear conformation was observed for the inhibitor N^1,N^{11}-bis(ethyl)norspermine (BE-3-3-3) (Bewley et al., 2006) and a bent conformation was reported for Spm (Hegde et al., 2007). In PpSSAT, the bound 1PE molecule mimicking Spm substrate adopts the bent conformation (Figure S10). Many of these interactions are water-mediated. The cavity surrounding the terminal part of Spm (comprising N^9 and N^{12} atoms) is less conserved and has a different shape (Figure S10). Indeed, the binding of the N^{12} atom of Spm mediated by His126 in hSSAT1 is replaced by the conserved glutamate in plant SSATs (Glu174 in PpSSAT). The two conserved Arg172 and Arg203 in plant SSATs (PpSSAT numbering), as well as Met196, protrude towards the terminal part of the substrate (Figure 4c,d). Both R203A and R172A mutations result in a loss of interaction with the carboxylate group of the amino acid substrate, and thus decreased affinity and activity (Table 5), in line with the observed interactions in the crystal structure.

Phylogenetic analysis of 60 plant SSATs revealed an interesting active-site difference. Lower plants and monocots possess Cys176, whereas dicots comprise a valine residue instead (Figure S8). The Cys176 appears to affect both polyamine binding as well as activity. Its side chain is H-bonded to Tyr138. Both residues establish water-mediated bonds with the N^1 and N^4 atoms of Spm, as manually modeled based on the 1PE molecule in the PpSSAT structure and with the N^6 atom Lys (Figure 4e,g). Although the side chain of Cys176 adopts different conformations in both structures, a direct interaction with the substrate was not observed. A hydrogen bond donor (such as tyrosine) near a cysteine residue is known to decrease its pK_a value (Bulaj et al., 1998), which suggests that C176 might exists as a thiolate anion at neutral pH. Its side chain can interact with the conserved water molecule that is bound to the substrate nitrogen (Figure 4g) and may thus facilitate the deprotonation step of the bound substrate mediated mainly by E140. Therefore, decreased activity of C176A and C176V mutants with Spm and their lower affinity to Spm can be explained only via disrupted water-mediated interactions and decreased deprotonation force.

Role of SSATs in mammals and plants

We confirmed that plant SSATs exhibit broad substrate specificity in extracts of *E. coli* cells overexpressing three plant *SSATs*. Indeed, we observed (i) the disappearance of the major putative substrates studied *in vitro*, namely DAP, Put, Spd, Spm, Lys and Orn, and (ii) the accumulation of the acetylated forms of amino-acids N^5-AcOrn and N^6-AcLys. The absence of the acetylated di- and polyamine-derivatives suggests their quick export outside the cells (the oxidative degradation via PAO cannot occur because of the absence of the *PAO* gene in *E. coli* genome). Excretion could be achieved by spermidine excretion transporter MdtJI (Higashi et al., 2008) or by PotE and CadB, which are known as putrescine–ornithine and cadaverine–lysine antiporters, respectively.

Similarly, constitutive or inducible *SSAT1* overexpression in mammalian cells leads to the reduction of Spm/Spd pools, whereas acSpm and acSpd are excreted. Moreover, polyamine metabolic flux, which is accelerated, leads to acCoA and malonyl-CoA depletion and in turn reduces the synthesis of fatty acids (Jänne et al., 2006; Pietilä et al., 1997; Vujcic et al., 2000). By contrast, mice *ssat1* knockouts displayed reduced polyamine metabolism, increased acetyl- and malonyl-CoA pools in white adipose cells and accumulation of body fat (Jell et al., 2007).

In the model plant Arabidopsis, SSATs were shown to catalyze the acetylation of various amino acids/polyamines. Indeed, a T-DNA insertion *nata1* line did not accumulate N^5-AcOrn and complementation with *35 S:NATA1* construct resulted in constitutive production of N^5-AcOrn (Adio et al., 2011). Transient expression of *NATA1* in tobacco led to formation of N^5-AcOrn and AcPut (Adio et al., 2011; Lou et al., 2016). The latter two compounds also accumulated

upon MeJA treatment in WT plants, and N^5-AcOrn was shown to reduce the reproduction of *Myzus persicae* (green peach aphid) (Adio et al., 2011, Lou et al., 2016). The stomatal-closing rate was accelerated in the *nata1* mutant, and the enzyme promoted stomata opening via acetylation of DAP, which antagonized the function of ABA (Jammes et al., 2014). Finally, silencing of *HSP90* genes coding for heat shock proteins (HSP) in *A. thaliana* resulted in elevated amounts of Spd, N^8-acSpd and N^1-acSpm, especially upon heat stress (Toumi et al., 2019). Consequently, the three *PAO* genes (*PAO1*, *PAO3* and *PAO5*), as well as the *NATA1* gene, were found to be upregulated.

Overall, our results emphasize the various substrates that can be acetylated by SSAT enzymes and the different roles that can be linked to their activity *in vivo* in mammals or plants.

EXPERIMENTAL PROCEDURES

Cloning, expression and purification of SSAT from *P. patens* and *Z. mays*

The total RNA from various maize organs (*Zea mays* cv. Cellux, Morseva) and from Physcomitrium ('Gransden 2004' strain) at the protonema stage was extracted using the RNAqueous kit and plant RNA isolation aid. The cDNA was synthesized using Superscript III RT and oligo dT primers (www.thermofisher.com). The sequence coding for PpSSAT (Pp3c5_21790V3.1, 645 bp) was amplified using gene-specific primers with *Nde*I and *Sal*I sites (5′-CAGTCATATGGCGATGGAAGGGACAC-3′, 5′-CACGTCGACTCAAAGCGCACACGCTTC-3′) and the Accuprime *Pfx* polymerase. ZmSSAT1 (Zm00001d048407; 678 bp) was amplified using gene-specific primers with *Nde*I and *Sal*I sites (5′-CATTCATATGGCGGCGGCGCCCTGCTC-3′, 5′-CACGTCGACCTATTCCGCAGCCGCAGCCT-3′). ZmSSAT2 (Zm00001d027703; 684 bp) was amplified using gene-specific primers with *Nhe*I and *Sal*I sites (5′-ATCGCTAGCATGGCGGCGCCGGCCAACTC-3′, 5′-ATTGTCGACCTACTCTGCAGCCTTCCCA-3′). The genes were further cloned into a pET28b vector from Merck (www.merckmillipore.com) and then transformed into Rosetta 2 (DE3) *E. coli* cells (www.neb.com). Protein production was carried out at 20°C overnight using 0.5 mM isopropylthio-β-galactoside. SSATs were purified on a Nickel-HiTrap IMAC FF column (https://www.cytivalifesciences.com) on a NGC Medium-Pressure Liquid Chromatography System (https://www.bio-rad.com) and further on a HiLoad 26/60 Superdex 200 column (www.gelifesciences.com) into 20 mM Tris–HCl buffer, pH 8.0, 300 mM NaCl. The yield after purification was about 12 mg per 100 ml of *E. coli* Rosetta 2 (DE3) cells.

Site-directed mutagenesis of PpSSAT

All mutants were cloned using tail-to-tail oriented phosphorylated primers, with the mutation being located at the 5′ end of one of the primers by a PCR reaction in 30 cycles. The following mutants were cloned: E140A (5′-P-GCGGATTTGTATGTGCGGAAAC-3′, 5′-P-GATGTAATATCCGCCCTTGG-3′), R172A (5′-P-GCAGTGGAATGGTGTGTGCTCG-3′, 5′-P-CCCAGCCCTGAGCTTCTTCGC-3′), M196A (5′-P-CCGGAGTGGCGCATCTGTCGTC-3′, 5′-P-TGCCACCTTCGCGCCAAGCCC-3′), R203A (5′-P-GCTCTAACAGGCGAGGCCTTGG-3′, 5′-P-ACAGATGCGCCACTCCGGCAT-3′) and C176A/C176V (5′-P-GCGGTGCTCGATTGGAATGTGAA-3′, 5′-P-GTTGTGCTCGATTGGAATGTGAA-3′, 5′-P-CCATTCCACTCGCCCAGCCCT-3′). The products were treated with the *Dpn*I, gel purified and ligated using the T4 DNA ligase from Promega (www.promega.com) and transformed into Rosetta 2 (DE3) *E. coli* cells.

Enzyme kinetics

SSAT activity was measured spectrophotometrically on an Agilent UV-visible spectrophotometer 8453 (www.agilent.com) at 30°C using a continuous 5,5′-dithiobis-(2-nitrobenzoic acid) (DTNB) assay. The reaction of DTNB with the thiol group of the CoA group yields a mixed disulfide and 2-nitro-5-thiobenzoate, which is followed at 412 nm (13.6 mM^{-1} cm^{-1}). Values for the blank containing the SSAT without the coenzyme were subtracted from reaction curves. The substrate screening was made in 100 mM Tris–HCl, pH 7.5 using 0.5 mM acCoA, 5 mM substrate, 0.5 mM DTNB, 2 mM EDTA and 5% glycerol. Kinetic constants K_m and V_{max} were determined using the PRISM, version 8.0 (www.graphpad.com). It should be noted that K_m and V_{max} for diamines and polyamines are rather apparent because the acetylation reaction could occur in two steps making the product of the first acetylation step, a possible substrate for the second acetylation step after leaving, rotating and re-entering the active site. pK_a values were calculated via MARVIN (https://chemaxon.com).

Affinity and thermal stability determination

The MST method was used to determine the binding affinity. PpSSAT and ZmSSAT2 were fluorescently labeled using the second generation RED-tris-NTA dye (www.nanotemper-technologies.com) using a 1:1 dye/protein molar ratio. The labeled protein was adjusted to 65 nM with phosphate-buffered saline buffer with 0.05% Tween. Measurements were performed in premium capillaries on a Monolith NT.115 instrument (www.nanotemper-technologies.com) at 30°C with 5 sec/30 sec/5 sec laser off/on/off times, respectively, with the excitation power set to 100%. Thermal stability was measured by the nano-differential scanning fluorimetry on Tycho NT.6 and Prometheus Panta instruments (www.nanotemper-technologies.com) in various buffers and in the presence of putative substrates and coenzyme in a range from 20 to 95°C and with a heating rate of 1°C min^{-1}, using Panta control software. Protein unfolding was measured by detecting the temperature-induced change in tryptophan fluorescence intensity at emission wavelengths of 330 and 350 ± 5 nm. The melting temperature was deduced from the maximum of the first derivative of the fluorescence ratios F_{350}/F_{330}. The turbidity was measured in the back reflection mode to identify the temperature at which the protein starts to aggregate.

Phylogenetic analysis

Amino acid alignment was performed with MUSCLE (Edgar, 2004), treated with GBLOCKS (Castresana, 2000) and the maximum likelihood phylogeny with bootstrap analysis was performed with PHYML, version 3.0 using LG amino acid replacement matrix (Guindon et al., 2010). Sequences were retrieved from UniProt (http://www.uniprot.org) and Phytozome 12 (https://phytozome.jgi.doe.gov), and expressed sequence tags from 'Green algal transcriptomes for phylogenetics and comparative genomics' (https://doi.org/10.6084/m9.figshare.1604778).

Quantitative PCR (qPCR) analysis

Moss was continuously grown in liquid Knop's medium and then exposed to 10 μM ABA, benzyl adenine or MeJA, 200 mM NaCl, 400 mM sorbitol and altered nitrogen content containing 10% (low)

and 200% nitrate (high) for 4 days. Heat stress was carried out at 37°C for 1 h, and cold stress was carried out for 5 h at 6°C. RNA was extracted by Trizol (www.thermofisher.com), transcribed in two independent reactions using a LunaScript RT SuperMix (www.neb.com), and the qPCR was performed using an RT Luna Universal Probe qPCR Master Mix (www.neb.com). *PpSSAT* primers (5′-ACCCTATCGACGATTCTGCAA-3′, 5′-CGAAGCCGACT GTTGTGTGA-3′) and the FAM-TAM probe (5′-CTTCAGGTCGCCGT CAACTGGCA-3′) were designed using PRIMER EXPRESS, version 3.0. Plasmid construct carrying the open reading frame was used for PCR efficiency determination. Cycle threshold values were normalized to moss *elongation factor 1α* and *β-actin* genes and amplification efficiency (Korasick et al., 2019).

Crystallization and structure determination

Crystallization conditions of purified PpSSAT at 11.4 mg ml^{-1} (20 mM Tris–HCl, pH 8.0, 100 mM NaCl) were screened using the PEGs II suite (www.qiagen.com) in the presence of 5 mM acCoA. Crystals were obtained in sitting drops in presence of 10% PEG 8000 and 10% PEG 1000. Crystals were transferred to a cryoprotectant solution (the mother liquor supplemented with 20% glycerol) and flash-frozen in liquid nitrogen. The crystals of the ternary complex with 20 mM Lys + 5 mM CoA were obtained using PpSSAT at 12 mg ml^{-1} in 0.2 M ammonium sulfate, 0.1 M trisodium citrate pH 5.6 and 15% PEG 4000. Diffraction data were collected at 100 K on the PROXIMA 2 beamline at the SOLEIL synchrotron (www.synchrotron-soleil.fr). Intensities were integrated using AUTOPROC (www.globalphasing.com) and XDS (Kabsch, 2010) and further reprocessed by STARANISO (Tickle et al., 2018). Data quality was assessed using the correlation coefficient $CC_{1/2}$ (Table S2). Molecular replacement was conducted with PHASER (Storoni et al., 2004) using the structure of SSAT2 from *Homo sapiens* (PDB 2BEI) (Han et al., 2006) as a search model. Models were refined with non-crystallographic symmetry restraints and TLS (i.e. translation, libration and screw-rotation) using BUSTER 2.10 (Bricogne et al., 2011) and with ligand occupancies set to 1. Electron density maps were evaluated using COOT (Emsley & Cowtan, 2004). Molecular graphics images were generated using PYMOL, version 1.8 (www.pymol.org). Structure models of ZmSSAT1 and ZmSSAT2 were constructed using ALPHAFOLD2 (Mirdita et al., 2022). The channel surface was calculated using HOLLOW (Ho & Gruswitz, 2008).

Polyamine and amino acid determination

All polyamines (as hydrochlorides) and amino acids were from Sigma-Aldrich (www.sigmaaldrich.com) except for norspermine, which was from ACROS (www.acros.com). Among acetyl derivatives, acPut and N^8-acSpd were from Santa Cruz Biotechnology (www.scbt.com), N^1-acSpm, N^1-acSpd and acAgm were from Cayman Chemical (www.caymanchem.com), N^6-acLys, N^2-acLys, N^5-acOrn, acnSpd were from Sigma-Aldrich, N^2-acOrn was from Biosynth Carbosynth (www.biosynth.com) and AcTryp was from TCI Chemicals (www.tcichemicals.com). Monoacetyl-DAP hydrochloride was synthesized using a procedure described for the synthesis of monoacetyl-Put hydrochloride (Tabor et al., 1964). Yield, 0.84 g (46%); m.p. 154–160°C; ^{1}H NMR (500 MHz, DMSO-d_6): δ 1.65 (2H, qui, J = 7.3 Hz, CH_2), 1.77 (3H, s, CH_3), 2.71 (2H, sextet, J = 6.7 Hz, CH_2), 3.04 (2H, q, J = 6.1 Hz, CH_2), 8.06 (3H, s(br), $NH4^+$), 8.10 (1H, t, J = 5.5 Hz, NH).

Polyamines and amino acids were quantified in accordance with previously described methods (Abdelhakim et al., 2022; Ćavar Zeljković et al., 2022). Briefly, pulverized sample material (3–5 mg) was mixed with 1 ml of 50% EtOH and sonicated for 10 min (https://bandelin.com). After centrifugation at 14 500 ***g***, the supernatant was transferred into the new vial and maintained at −20°C until analysis. For the analysis of free amino acids and acetylated polyamines, an aliquot of 200 μl was evaporated to dryness and then re-dissolved into 50 μl of the mobile phase, consisting of 20-mM ammonium formate, pH 3.0 (Component A) and 0.1% formic acid in ACN (Component B). LC–MS analysis was performed on Nexera X2 UHPLC coupled with MS-8050 (www.shimadzu.eu.com). Chromatographic separation was performed on an Acquity UPLC BEH AMIDE column (50 × 2.1 mm; 1.7 μm particle size) (www.waters.com) with an appropriate pre-column. Another aliquot of 200 μl was used for the determination of free polyamines, which were benzoylated before analysis. LC–MS analysis was performed using the same instrument described above. Separation was performed on an Acquity UPLC C18 BEH column (50 × 2.1 mm; 1.7 μm particle size) with an appropriate pre-column, and the mobile phase consisted of a mixture of 15 mM formic acid (Component A), pH 3.0, and methanol (Component B).

ACCESSION NUMBERS

The atomic coordinates and structure factors have been deposited in the Protein Data Bank (www.wwpdb.org) under accession codes 7ZHC for PpSSAT in complex with acCoA and PEG mimicking spermine and 7ZKT for PpSSAT in the ternary complex with CoA and Lys.

AUTHOR CONTRIBUTIONS

MK, DK and SM designed the research. JB, EH, JF, DJK and MK prepared enzyme variants and their mutants, as well as measured enzyme properties with kinetics and real-time PCR. SĆZ, PT, JN and NDD were involved in measurements of polyamine and amino acids levels and acetyl-derivatives. DK, PB, SM, AV and FJ performed the crystallographic study and analyzed the crystal structures. MK, DK and SM wrote the paper. All authors reviewed the results and approved the final version of the manuscript submitted for publication.

ACKNOWLEDGEMENTS

This work was supported by Junior grant no. JG_2020_001 and IGA_PrF_2022_007 from Palacký University, grant no. 21-07661 S from the Czech Science Foundation, the ERDF project 'Plants as a tool for sustainable global development' (No. CZ.02.1.01/0.0/0.0/16_019/0000827) and 'Improving Schematics of Doctoral Student Grant Competition and their Pilot Implementation' (No. CZ.02.2.69/0.0/0.0/19_073/0016713, namely grant DSGC-2021-0158), from the Ministry of Education, Youth and Sports of the Czech Republic, as well as by project No. RO0423 (Sustainable systems and technologies, improving crop production for a higher quality of production of food, feed and raw materials, under conditions of changing climate), the Ministry of Agriculture, Czech Republic. This work benefited from the I2BC crystallization platforms supported by FRISBI ANR-10-INSB-05-01. We acknowledge SOLEIL for the provision of synchrotron radiation facilities (proposal IDs 20191181 and 20210831) in using PROXIMA beamlines and we thank the staff for their assistance with respect to using the beamlines.

CONFLICT OF INTEREST

The authors declare no conflict of interest.

DATA AVAILABILITY STATEMENT

All relevant data can be found within the manuscript and the supporting materials.

SUPPORTING INFORMATION

Additional Supporting Information may be found in the online version of this article.

Table S1. Sequence identity between maize, moss and human SSAT enzymes.

Table S2. Data collection and refinement statistics of PpSSAT complexes.

Table S3. List of sequences used for residue conservation in the coenzyme binding site.

Figure S1. Molecular properties of three plant SSATs.

Figure S2. Analysis of reaction products of Lys and Orn incubated with PpSSAT overnight.

Figure S3. Coenzyme affinity and kinetics of SSATs.

Figure S4. PpSSAT affinity for substrates and inhibition screening.

Figure S5. Gene expression of *SSAT* in moss *Physcomitrium patens* under various stresses.

Figure S6. Sequence alignment of the three plant SSATs studied in the present study and two human SSATs.

Figure S7. Electron density evidence for acCoA and substrate ligands in PpSSAT structures.

Figure S8. Analysis of active-site variants of PpSSAT.

Figure S9. Maize SSAT models and active site differences.

Figure S10. A possible reaction mechanism and substrate cavity in plant SSATs.

REFERENCES

Abdelhakim, L.O.A., Mendanha, T., Palma, C.F.F., Vrobel, O., Štefelová, N., Ćavar Zeljković, S. *et al.* (2022) Elevated CO_2 improves the physiology but not the final yield in spring wheat genotypes subjected to heat and drought stress during anthesis. *Frontiers in Plant Science*, **13**, 824476.

Adio, A.M., Casteel, C.L., De Vos, M., Kim, J.H., Joshi, V., Li, B. *et al.* (2011) Biosynthesis and defensive function of Nδ-acetylornithine, a jasmonate-induced Arabidopsis metabolite. *Plant Cell*, **23**, 3303–3318.

Ahou, A., Martignago, D., Alabdallah, O., Tavazza, R., Stano, P., Macone, A. *et al.* (2014) A plant spermine oxidase/dehydrogenase regulated by the proteasome and polyamines. *Journal of Experimental Botany*, **65**, 1585–1603.

Batista-Silva, W., Heinemann, B., Rugen, N., Nunes-Nesi, A., Araújo, W.L., Braun, H.P. *et al.* (2019) The role of amino acid metabolism during abiotic stress release. *Plant, Cell & Environment*, **42**, 1630–1644.

Bewley, M.C., Graziano, V., Jiang, J., Matz, E., Studier, F.W., Pegg, A.E. *et al.* (2006) Structures of wild-type and mutant human spermidine/spermine N^1-acetyltransferase, a potential therapeutic drug target. *Proceedings of the National Academy of Sciences of the United States of America*, **103**, 2063–2068.

Bolkenius, F.N. & Seiler, N. (1981) Acetylderivatives as intermediates in polyamine catabolism. *The International Journal of Biochemistry*, **13**, 287–292.

Bricogne, G., Blanc, E., Brandl, M., Flensburg, C., Keller, P., Paciorek, W. *et al.* (2011) *BUSTER version 2.1.0*. Cambridge, UK: Global Phasing Ltd.

Bulaj, G., Kortemme, T. & Goldenberg, D.P. (1998) Ionization-reactivity relationships for cysteine thiols in polypeptides. *Biochemistry*, **37**, 8965–8972.

Castresana, J. (2000) Selection of conserved blocks from multiple alignments for their use in phylogenetic analysis. *Molecular Biology and Evolution*, **17**, 540–552.

Cavallini, D., Ricci, G., Duprè, S., Pecci, L., Costa, M., Matarese, R.M. *et al.* (1991) Sulfur-containing cyclic ketimines and imino acids. A novel family of endogenous products in the search for a role. *European Journal of Biochemistry*, **202**, 217–223.

Ćavar Zeljković, S., Aucique-Perez, C.E., Stefelova, N. & De Diego, N. (2022) Optimizing growing conditions for hydroponic farming of selected medicinal and aromatic plants. *Food Chemistry*, **375**, 131845.

Coleman, C.S., Huang, H. & Pegg, A.E. (1996) Structure and critical residues at the active site of spermidine/spermine N1-acetyltransferase. *Biochemical Journal*, **316**, 697–701. https://doi.org/10.1042/bj3160697

Coleman, C.S., Stanley, B.A., Jones, A.D. & Pegg, A.E. (2004) Spermidine/spermine-N^1-acetyltransferase-2 (SSAT2) acetylates thialysine and is not involved in polyamine metabolism. *The Biochemical Journal*, **384**, 139–148.

Della Ragione, F. & Pegg, A.E. (1983) Studies of the specificity and kinetics of rat liver spermidine/spermine N^1-acetyltransferase. *The Biochemical Journal*, **213**, 701–706.

Edgar, R.C. (2004) MUSCLE: multiple sequence alignment with high accuracy and high throughput. *Nucleic Acids Research*, **32**, 1792–1797.

Emsley, P. & Cowtan, K. (2004) Coot: model-building tools for molecular graphics. *Acta Crystallographica. Section D, Biological Crystallography*, **60**, 2126–2132.

Federico, R., Ercolini, L., Laurenzi, M. & Angelini, R. (1996) Oxidation of acetylpolyamines by maize polyamine oxidase. *Phytochemistry*, **43**, 339–341.

Forouhar, F., Lee, I.S., Vujcic, J., Vujcic, S., Shen, J., Vorobiev, S.M. *et al.* (2005) Structural and functional evidence for *Bacillus subtilis* PaiA as a novel N^1-spermidine/spermine acetyltransferase. *The Journal of Biological Chemistry*, **280**, 40328–40336.

Guindon, S., Dufayard, J.F., Lefort, V., Anisimova, M., Hordijk, W. & Gascuel, O. (2010) New algorithms and methods to estimate maximum-likelihood phylogenies: assessing the performance of PhyML 3.0. *Systematic Biology*, **59**, 307–321.

Hamana, K. & Matsuzaki, S. (1985) Distinct difference in the polyamine compositions of bryophyta and pteridophyta. *Journal of Biochemistry*, **97**, 1595–1601.

Han, B.W., Bingman, C.A., Wesenberg, G.E. & Phillips, G.N., Jr. (2006) Crystal structure of Homo sapiens thialysine Nε-acetyltransferase (HsSSAT2) in complex with acetyl coenzyme A. *Proteins*, **64**, 288–293.

Hegde, S.S., Chandler, J., Vetting, M.W., Yu, M. & Blanchard, J.S. (2007) Mechanistic and structural analysis of human spermidine/spermine N^1-acetyltransferase. *Biochemistry*, **46**, 7187–7195.

Hennion, F., Bouchereau, A., Gauthier, C., Hermant, M., Vernon, P. & Prinzing, A. (2012) Variation in amine composition in plant species: how it integrates macroevolutionary and environmental signals. *American Journal of Botany*, **99**, 36–45.

Hickman, A.B., Namboodiri, M.A., Klein, D.C. & Dyda, F. (1999) The structural basis of ordered substrate binding by serotonin N-acetyltransferase: enzyme complex at 1.8 a resolution with a bisubstrate analog. *Cell*, **97**, 361–369.

Higashi, K., Ishigure, H., Demizu, R., Uemura, T., Nishino, K., Yamaguchi, A. *et al.* (2008) Identification of a spermidine excretion protein complex (MdtJI) in *Escherichia coli*. *Journal of Bacteriology*, **190**, 872–878.

Ho, B.K. & Gruswitz, F. (2008) HOLLOW: generating accurate representations of channel and interior surfaces in molecular structures. *BMC Structural Biology*, **8**, 49.

Jammes, F., Leonhardt, N., Tran, D., Bousserouel, H., Véry, A.A., Renou, J.P. *et al.* (2014) Acetylated 1,3-diaminopropane antagonizes abscisic acid-mediated stomatal closing in Arabidopsis. *The Plant Journal*, **79**, 322–333.

Jänne, J., Alhonen, L., Pietilä, M., Keinänen, T.A., Uimari, A., Hyvönen, M.T. *et al.* (2006) Genetic manipulation of polyamine catabolism in rodents. *Journal of Biochemistry*, **139**, 155–160.

Jell, J., Merali, S., Hensen, M.L., Mazurchuk, R., Spernyak, J.A., Diegelman, P. *et al.* (2007) Genetically altered expression of spermidine/spermine N^1-acetyltransferase affects fat metabolism in mice via acetyl-CoA. *The Journal of Biological Chemistry*, **282**, 8404–8413.

Joghee, N.N. & Jayaraman, G. (2014) Metabolomic characterization of halophilic bacterial isolates reveals strains synthesizing rare diaminoacids under salt stress. *Biochimie*, **102**, 102–111.

Jun, D.Y., Rue, S.W., Han, K.H., Taub, D., Lee, Y.S., Bae, Y.S. *et al.* (2003) Mechanism underlying cytotoxicity of thialysine, lysine analog, toward human acute leukemia Jurkat T cells. *Biochemical Pharmacology*, **66**, 2291–2300.

Kabsch, W. (2010) XDS. *Acta Crystallographica. Section D, Biological Crystallography*, **66**, 125–132.

Kakegawa, T., Guo, Y., Chiba, Y., Miyazaki, T., Nakamura, M., Hirose, S. *et al.* (1991) Effect of acetylpolyamines on in vitro protein synthesis and on the growth of a polyamine-requiring mutant of *Escherichia coli*. *Journal of Biochemistry*, **109**, 627–631.

Kim, D.W., Watanabe, K., Murayama, C., Izawa, S., Niitsu, M., Michael, A.J. *et al.* (2014) Polyamine Oxidase5 regulates Arabidopsis growth through thermospermine oxidase activity. *Plant Physiology*, **165**, 1575–1590.

Kiyota, E., Pena, I.A. & Arruda, P. (2015) The saccharopine pathway in seed development and stress response of maize. *Plant, Cell & Environment*, **38**, 2450–2461.

Kopečný, D., Končitíková, R., Tylichová, M., Vigouroux, A., Moskalíková, H., Soural, M. *et al.* (2013) Plant ALDH10 family: identifying critical residues for substrate specificity and trapping a thiohemiacetal intermediate. *The Journal of Biological Chemistry*, **288**, 9491–9507.

Korasick, D.A., Končitíková, R., Kopečná, M., Hájková, E., Vigouroux, A., Moréra, S. *et al.* (2019) Structural and biochemical characterization of aldehyde dehydrogenase 12, the last enzyme of proline catabolism in plants. *Journal of Molecular Biology*, **431**, 576–592.

Landry, J. & Sternglanz, R. (2003) Yeast Fms1 is a FAD-utilizing polyamine oxidase. *Biochemical and Biophysical Research Communications*, **303**, 771–776.

Lou, Y.R., Bor, M., Yan, J., Preuss, A.S. & Jander, G. (2016) Arabidopsis NATA1 acetylates putrescine and decreases defense-related hydrogen peroxide accumulation. *Plant Physiology*, **171**, 1443–1455.

Lu, L., Berkey, K.A. & Casero, R.A., Jr. (1996) RGFGIGS is an amino acid sequence required for acetyl coenzyme A binding and activity of human spermidine/spermine N^1acetyltransferase. *The Journal of Biological Chemistry*, **271**, 18920–18924.

Mamont, P.S., Seiler, N., Siat, M., Joder-Ohlenbusch, A.M. & Knödgen, B. (1981) Metabolism of acetyl derivatives of polyamines in cultured polyamine-deficient rat hepatoma cells. *Medical Biology*, **59**, 347–353.

Mattioli, R., Pascarella, G., D'Incà, R., Cona, A., Angelini, R., Morea, V. *et al.* (2022) Arabidopsis N-acetyltransferase activity 2 preferentially acetylates 1,3-diaminopropane and thialysine. *Plant Physiology and Biochemistry*, **170**, 123–132.

McCloskey, D.E. & Pegg, A.E. (2003) Properties of the spermidine/spermine N^1-acetyltransferase mutant L156F that decreases cellular sensitivity to the polyamine analogue N^1,N^11-bis(ethyl)norspermine. *The Journal of Biological Chemistry*, **278**, 13881–13887.

Mirdita, M., Schütze, K., Moriwaki, Y., Heo, L., Ovchinnikov, S. & Steinegger, M. (2022) ColabFold: making protein folding accessible to all. *Nature Methods*, **19**, 679–682.

Montemayor, E.J. & Hoffman, D.W. (2008) The crystal structure of spermidine/spermine N^1-acetyltransferase in complex with spermine provides insights into substrate binding and catalysis. *Biochemistry*, **47**, 9145–9153.

Müller, B., Fastner, A., Karmann, J., Mansch, V., Hoffmann, T., Schwab, W. *et al.* (2015) Amino acid export in developing Arabidopsis seeds depends on UmamiT facilitators. *Current Biology*, **25**, 3126–3131.

Neuwald, A.F. & Landsnan, D. (1997) GCN5-related histone N-acetyltransferases belong to a diverse superfamily that includes the yeast SPT10 protein. *Proceedings of the National Academy of Sciences of the United States of America*, **51**, 154–155.

Pegg, A.E. (2008) Spermidine/spermine-N(1)-acetyltransferase: a key metabolic regulator. *American Journal of Physiology. Endocrinology and Metabolism*, **294**, E995–E1010.

Perez-Leal, O. & Merali, S. (2012) Regulation of polyamine metabolism by translational control. *Amino Acids*, **42**, 611–617.

Pietilä, M., Alhonen, L., Halmekytö, M., Kanter, P., Jänne, J. & Porter, C.W. (1997) Activation of polyamine catabolism profoundly alters tissue polyamine pools and affects hair growth and female fertility in transgenic mice overexpressing spermidine/spermine N^1-acetyltransferase. *The Journal of Biological Chemistry*, **272**, 18746–18751.

Scheibner, K.A., De Angelis, J., Burley, S.K. & Cole, P.A. (2002) Investigation of the roles of catalytic residues in serotonin N-acetyltransferase. *The Journal of Biological Chemistry*, **277**, 18118–18126.

Storoni, L.C., McCoy, A.J. & Read, R.J. (2004) Likelihood-enhanced fast rotation functions. *Acta Crystallographica. Section D, Biological Crystallography*, **60**, 432–438.

Tabor, C.W., Tabor, H. & Bachrach, U. (1964) Identification of the aminoaldehydes produced by the oxidation of spermine and spermidine with purified plasma amine oxidase. *The Journal of Biological Chemistry*, **239**, 2194–2203.

Tavladoraki, P., Cona, A., Federico, R., Tempera, G., Viceconte, N., Saccoccio, S. *et al.* (2012) Polyamine catabolism: target for antiproliferative therapies in animals and stress tolerance strategies in plants. *Amino Acids*, **42**, 411–426.

Tickle, I.J., Flensburg, C., Keller, P., Paciorek, W., Sharff, A., Vonrhein, C. *et al.* (2018) *STARANISO*. Cambridge, UK: Global Phasing Ltd. http://staraniso.globalphasing.org/cgi-bin/staraniso.cgi

Toumi, I., Pagoulatou, M.G., Margaritopoulou, T., Milioni, D. & Roubelakis-Angelakis, K.A. (2019) Genetically modified heat shock Protein90s and polyamine oxidases in Arabidopsis reveal their interaction under heat stress affecting polyamine acetylation, oxidation and homeostasis of reactive oxygen species. *Plants*, **8**, 323.

Uemura, T., Yerushalmi, H.F., Tsaprailis, G., Stringer, D.E., Pastorian, K.E., Hawel, L., 3rd *et al.* (2008) Identification and characterization of a diamine exporter in colon epithelial cells. *The Journal of Biological Chemistry*, **283**, 26428–26435.

Vujcic, S., Halmekyto, M., Diegelman, P., Gan, G., Kramer, D.L., Janne, J. *et al.* (2000) Effects of conditional overexpression of spermidine/spermine N^1-acetyltransferase on polyamine pool dynamics, cell growth, and sensitivity to polyamine analogs. *The Journal of Biological Chemistry*, **275**, 38319–38328.

Wallace, H.M., Fraser, A.V. & Hughes, A. (2003) A perspective of polyamine metabolism. *The Biochemical Journal*, **376**, 1–14.

Winter, G., Todd, C.D., Trovato, M., Forlani, G. & Funck, D. (2015) Physiological implications of arginine metabolism in plants. *Frontiers in Plant Science*, **6**, 534.

Yamaguchi, K., Takahashi, Y., Berberich, T., Imai, A., Miyazaki, A., Takahashi, T. *et al.* (2006) The polyamine spermine protects against high salt stress in *Arabidopsis thaliana*. *FEBS Letters*, **580**, 6783–6788.

Zhao, F., Song, C.P., He, J. & Zhu, H. (2007) Polyamines improve K+/Na+ homeostasis in barley seedlings by regulating root ion channel activities. *Plant Physiology*, **145**, 1061–1072.

Zhu, Y.Q., Zhu, D.Y., Yin, L., Zhang, Y., Vonrhein, C. & Wang, D.C. (2006) Crystal structure of human spermidine/spermine N^1-acetyltransferase (hSSAT): the first structure of a new sequence family of transferase homologous superfamily. *Proteins*, **63**, 1127–1131.